OPTIMIZATION AND CHARACTERIZATION OF BI-DETECTOR COINCIDENCE BETA-RAY SPECTROMETER

BY

RUOYU SUN, B.Sc.

A THESIS

SUBMITTED TO THE DEPARTMENT OF RADIATION SCIENCE

AND THE SCHOOL OF GRADUATE STUDIES

OF MCMASTER UNIVERSITY

IN PARTIAL FULFILMENT OF THE REQUIREMENTS

FOR THE DEGREE OF

MASTER OF SCIENCE

MASTER OF SCIENCE (2021) McMaster University

(Medical Physics) Hamilton, Ontario, Canada

TITLE: Optimization and Characterization of Bi-detector Coincidence Beta-ray Spectrometer

AUTHOR: Ruoyu Sun, B.Sc. (Medical Physics)

McMaster University, Hamilton, Ontario, Canada

SUPERVISOR: Dr. Soo Hyun Byun

NUMBER OF PAGES: xi,72

Abstract

With the recent change of the equivalent dose limit for the lens of eyes from 150 to 20 mSv/yr., averaged over 5 years, it is of great importance to investigate the beta-ray spectrum in the maintenance areas of the nuclear power plants, where workers are exposed to mixed beta-gamma fields. A beta-ray spectrometer consisting of a thin silicon detector and a plastic scintillator has been developed, which can accept only beta detection events while rejecting gamma events via coincidence. Based on the spectroscopy system that has been built, a comprehensive upgrade of software and hardware has been conducted. The data acquisition software MC2 was replaced with CoMPASS, developed by CAEN to achieve higher stability and functionality. Optimal shaping parameters and coincidence time window were determined by instruction and sample tests. The fast event signal from the plastic scintillator does not provide enough energy information. Therefore, three approaches were executed, including adding a capacitor, adding a preamplifier, and changing the digital pulse processor to solve the problem. The method of changing digitizer was accepted as the final solution to obtain the best spectrum through benchmark tests. The experimental measurements characterized the response of the beta-ray coincidence spectrometer under the mixed beta/gamma radiation field with a various count rate ratio from 0.00625 to 0.8. Experimental result shows excellent and stable performance of the detector system under a higher beta to gamma ratio. Gamma contribution of the coincidence spectrum, especially in low energy region, significantly increased when beta count rate was controlled to a minor level. Monte Carlo simulations are also carried out using the MCNP6 code to validate the measurements.

Acknowledgment

It is never too much to express my gratitude for all the help and support I received during my master's studies. The COVID-19 pandemic profoundly changed our lives and composed the majority time of me being a graduate student. I am incredibly grateful for the work of all the people that help overcome the difficulties.

First of all, I would like to express my sincere gratitude to Dr. Soo Hyun Byun as an ideal teacher, mentor, and thesis supervisor, offering advice and encouragement with a perfect blend of insight and humor. Dr. Byun has been an inspiration as I hurdled through the path of this Master's degree. It is my honor and fortune to be your student. I would also like to thank my committee members Dr. Jovica Atanackovic and Dr. Andrei Hanu, for their guidance and insightful advice. Thank you for taking the time to review my project and oversee my defense.

I would like to give a special thank to Mr. Xingzhi Cheng for his enthusiastic help in academics and life. You have been my goal and one of my best friends since my undergraduate. It would be a harder and thornier road without your experience and support. I would like to thank Ms. Xin Tong and Ms. Laila Omar-nazir for sharing their valuable experiences and helping me get started with the project. Thank everyone in Byun's group for providing me advises and helps when I was seeking it. Also, thank all my colleagues in RadGrad for all the cheerful time spending with you.

I am grateful for my parents, whose constant love and support keep me motivated and confident. Thank all my friends for your continuous encouragement and relaxation place provided. I would not be here without you.

Contents

List of Figures

List of Tables

Chapter 1 Introduction

1.1 Equivalent dose limit change for the lens of the eye

Excessive ionizing radiation dose may cause many harmful effects and irreversible diseases. Harmful effects caused by radiation are usually divided into two categories: deterministic effects and stochastic effects. A stochastic effect is an adverse health effect after a relatively low exposure. The stochastic effect occurs with a probability proportional to the dose received, without a dose threshold. The ultimate result of a stochastic effect is usually cancer and hereditary effects, whose severity usually does not depend on the dose received. A deterministic effect, in contrast, is an adverse health effect caused by intense radiation exposure. A typical characteristic of deterministic effect is the threshold above which the level of harm increases as the dose increases. Deterministic effects are based on tissue damage, and the severity increase with the increase of dose level. Examples of deterministic effects include radiation-induced skin burns, acute radiation syndrome, and cataract formation. [1]

The lens of the eye is one of the most radiosensitive organs. Cataract formation has long been considered a major oscular complication associated with excessive ionizing radiation exposure. [2] Various theories have been proposed to explain how radiation induces cataracts, but no consensus exists on the exact mechanisms of cataract induction and progression. Cellular damage leading to cataract formation can occur from radiation interactions with both DNA and proteins. [3] It is believed that radiation exposure is inversely related to the latency period to the onset of cataracts, varying from years to decades. [4,5]

As a typical deterministic effect, cataract formation should have a clear threshold, below which the health effect is neglectable. Practically, the threshold is defined as the dose resulting in a 1% incidence of specified tissue or organ reactions. The dose limit to the eye lens can be set from the threshold for various groups of

people who may be potentially exposed to radiation fields. The International Commission on Radiological Protection (ICRP) is an independent international organization that provides guidance and recommendation in various aspects of health physics. The annual occupational dose limit is one of the most crucial quantities for medical and industrial staff. With the advancement of science and the conduct of new research over the last few decades, the recommended dose limit from the ICRP has also been updated several times.

In 1977, the dose limit for the eyes' lens was first evaluated from ICRP publication 26. It was determined that a 15 Sv equivalent dose accumulated in an occupational lifetime would unlikely induce vision-impairing opacities. The first annual dose limit for the lens of the eyes was set at 300 mSv. This initial dose limit, however, did not last a long time. In ICRP publication 41, released in 1984, the annual dose limit for the lens of the eye was reduced to 150 mSv. The new estimated threshold for vision-impairing cataracts was 5 Gy and 8 Gy for a single acute exposure and fractionated/protracted exposures, respectively. The dose limit stayed at the same level for the next three decades through the evaluations in 1991 and 2007. However, in publication 103 released in 2007, it is noted that new data related to low dose exposure and cataract formation is forthcoming. [4]

In 2012, the detailed investigation result was announced in publication 118. The threshold of cataract formation decreased 10-fold to 0.5 Gy for both acute and protracted exposure. The recommended equivalent dose limit to the eye was subsequently lowered from 150 mSv per year and is now identical to effective dose limits; 20 mSv per year, averaged over five years, with a maximum exposure of 50 mSv in a single year. [6] The changing of dose limit was based on the new fundings in radiation-induced cataracts under low dose exposure. In earlier epidemiological studies, the follow-up of minor lens changes induced by radiation or visual disability requiring cataract surgery is insufficient due to the long latency period. Better technology detecting, quantifying, and documenting early radiation-associated lens changes and more precise dosimetry are essential factors contributing to the advancement. [6, 7]

1.2 Determination of dose equivalent under beta/gamma mixed field

The Canadian Nuclear Safety Commission (CNSC) implanted the recommended new lens of the eyes dose limit from ICRP, starting from Jan. 1, 2021. The changing dose limit applies to all nuclear energy workers (NEW) in the country, increasing the financial expense. For most NEW who have an annual dose of less than 10 mSv and where the eyes are not preferentially exposed to radiation during work activities, the modification of work practices is not required as the current radiation protection programs are sufficiently robust. [8] There are three types of workers who may receive significant routine doses to the lens of the eyes. Those are: 1) the workers that received relatively uniform whole body penetrating radiation fields; 2) the workers that received a highly non-uniform radiation field that lens of the eye may be preferentially exposed and 3) the workers exposed to weakly penetrating radiation, such as beta particles or low-energy photons that may have significant dose contribution to the lens of the eye. Therefore, this project is focused on the beta/gamma radiation field. There are reasonable reasons to exclude other types of particles. Alpha particles and other high LET radiation do not need to be considered a hazard for the eye lens, as their range in tissue is highly limited. The access to neutron exposure is complicated; however, the neutron is unlikely to contribute to eye dose significantly. The limit for the effective dose is usually reached far before the dose limit for the eye lens under the neutron fields. The energy of beta particles in this project is focused on the range from 700 keV to 3 MeV. Beta particles with energies lower than 700 keV would not be able to penetrate the lens of the eye. [7]

The operational quantity personal dose equivalent $H_p(d)$ is defined by dose equivalent at the depth d, in mm, under the body's position that dosimeter is worn. A depth of 0.07 mm is chosen to measure the skin dose of low penetrating

radiation. On the contrary, a depth of 10 mm is chosen to measure the effective dose of strong penetrating radiation. As for the dose equivalent toward the lens of the eye, a depth of 3 mm would be the optimal choice. Therefore, to measure the equivalent dose to the lens of the eye, the most direct and accurate method would be measuring dose equivalent in the depth of 3 mm $H_p(3)$ with the dosimeter worn at the position as close as possible to the eye. However, the optimal method would be impractical as the dosimeter designed for $H_p(3)$ was unavailable in many countries. Therefore, a dosimeter that measures other quantities may be used. The dosimeter for equivalent dose in the depth of 0.07 mm, $H_p(0.07)$, calibrated with the appropriate phantom, is usually considered as a conservative choice to measure dose for the lens of the eye. However, the performance of the dosimeter under beta/gamma mixed field could be incredibly inaccurate in this case, and the eye lens dose can be overestimated by up to a factor of 550. [9] When radiation fields in the workplace are known, estimating the eye lens dose Hp(3) from the dosimeter calibrated in terms of $H_p(0.07)$ or $H_p(10)$ is also achievable.

Thermoluminescent dosimeters (TLDs) are the dosimeter widely used in nuclear industries to monitor the external dose. A particular algorithm can be applied to TLDs to extract dose information, including the contribution of beta radiation to the total dose. The body dosimeter used in Ontario Power Generation (OPG) and Bruce Power (BP) consists of 4 Harshaw TLD-700 elements, made of thermo-luminescent material 7LiF:Mg,Ti can access both personal dose equivalent, Hp(0.07) or Hp(10). [11] The estimated eye lens dose would be inaccurate without knowing about the existing radiation field in various workplaces of the reactor.

The radiation field in the CANDU reactor is complicated. The coolant of the heat transport system could be contaminated with radionuclides from different sources. The most common radionuclides are Cs-137, Sr/Y-90 as fission products, Co-60, Sb-204 as the activation products. The workers come in close contact with residual radionuclide for inspection and maintenance services during

the unit outrage. Such work potentially exposed to high fluence rate of beta particle and photon usually be considered high hazard work and could potentially produce a significant dose to the lens of the eye. [12] The project's motivation would be to collect the beta information from the mixed beta/gamma radiation field.

1.3 Previous work

Since 2016, several projects have been started to collect radiation field information at the CANDU reactor. The lanthanum bromide detector was used to obtain the gamma fluence spectrum by A Laranjeiro.[13] At the same time, F. Bohra performed beta spectrometry using a plastic scintillator detector. [14] However, the plastic scintillator detector is too sensitive for both beta and gamma events. Thus, the pure beta spectrum could not be directly separated from the mixed field of beta particles and photons if only a plastic scintillator were used. The data analysis is complicated to extract the beta event spectrum. Specifically, the gamma contribution estimated by the gamma fluence spectrum obtained lanthanum bromide detector was subtracted from the plastic scintillator response. The method relies on independent data from two detectors and could potentially be inaccurate. Most importantly, the post-analysis process is complicated and does not allow for the real-time display of the beta spectrum during data collection at CANDU reactors.

To separate a more accurate beta spectrum and reject gamma events to the utmost extent, L. Omar-Nazir posed and successfully constructed a beta-ray coincidence spectroscopy system with silicon-plastic scintillator detector.[15] Monte Carlo simulations and experimental measurement with nuclides including Co-60, Cs-137, Sr/Y-90, and Ti-204 were performed to characterize the response of the beta-ray coincidence spectroscopy system.

1.4 Project Goal

The coincidence beta spectroscopy uses a silicon detector in conjunction with a plastic scintillator detector. Fig. 1.1 illustrates the probable interactions of gamma and beta particles with a Si-plastic scintillator coincidence spectrometer. As depicted in Figure. 1.1, the underlying principle is that gamma photons interact only with the plastic scintillator. In contrast, beta particles interact with both detectors or only with the Si detector, enabling us to reject the gamma detection events by the coincidence technique.

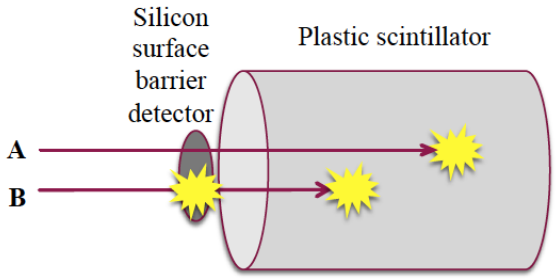

Figure 1.1 Most probable interactions of gamma and beta particles with a Si-plastic scintillator coincidence spectrometer. (A: gamma photon, B: beta particle)

Based on the system that has been built, a comprehensive upgrade of software and hardware has been conducted. Upgraded data acquisition software, digitizer, and preamplifier showed a better performance in various aspects. Further experimental measurements were designed to characterize the performance under a mixed beta/gamma radiation field.

Chapter 2 Beta-ray spectrometer system

2.1 System components

Multiple components are used in the beta-ray spectrometer system. These components include a thin silicon surface barrier detector, a plastic scintillator, a CAEN manufactured high voltage power supply, a CAEN manufactured preamplifier power supply, and a CAEN manufactured digital pulse processor. Finally, a laptop with specific software was used to acquire and analyze the data. Figure 2.1 below shows how the components are connected to the system.

Figure 2.1 Beta-ray spectrometers system. Labeled component: 1 Plastic scintillator detector, 2 Silicon SBD detector, 3 Charge sensitive preamplifier, 4 High voltage supply, 5 Digital pulse processor, 6 Preamplifier power supply, 7 Data acquisition laptop

2.1.1 Plastic scintillator detector

The plastic scintillator detector provided by Eljen Technology (model number M550-20x8-1) consists of several parts, including the EJ-204 plastic scintillator within the detector and an acrylic light guide. Both parts are cylindrical with a 5 cm diameter and 2 cm thickness. Following the plastic scintillator and light guide is a 5 cm diameter Hamamatsu R7724 photomultiplier tube.

The EJ-204 plastic scintillator (Eljen Technology, model number 204) is a cylindrical part with a light output of 68%, a scintillation efficiency of 10400 photons per 1 MeV electron, a rise time of 0.7 ns, and a decay time of 1.8 ns. [16] Compared to other plastic scintillator models from Eljen technology, EJ 204 is the perfect choice for this project due to having the fastest rise/decay time, highest efficiency, and shortest pulse width with a pulse full-width half maximum of 2.2 ns. Since the pulse width is inversely proportional to the energy resolution, the EJ-204 provides the highest resolution compared to other models.

2.1.2 Silicon Surface Barrier detector

The silicon surface detector (SBD) provided by Ortec (model number TD-015-050-100) is a planar totally depleted semiconductor detector with an active area of 50 mm^2 and a depletion depth of 100 μm.[17] This detector is placed in front of the plastic scintillator detector. High-energy particles will pass through the detector if the depletion depth is too thin, resulting in low interaction probability. However, if the depletion depth is too thick, some low-energy particles will be absorbed by the detector and not be detected by the plastic scintillator. In either case, there would be event loss in the silicon or plastic scintillator spectrum. Therefore, an optimal depletion depth to avoid both situations would be 100 μm.

Due to the surface area of the SBD being smaller than the diameter of the plastic scintillator, a 3D-printed plastic holder had to be used. This plastic holder is fixed to the front of the plastic scintillator detector and holds up the SBD. The silicon detector is connected to the charge-sensitive preamplifier by the microdot cable.

2.1.3 Charge sensitive preamplifier

The charge-sensitive preamplifier (model number A1422) provided by CEAN is a single channel preamplifier with a gain of 45 mV/MeV and an independent power supply. The preamplifier is only used for the silicon detector, and the side of the amplifier labeled “detector in” is connected to the cable with a BNC connector, while the other end of the cable is a microdot connector with a silicon detector.

2.1.4 High voltage supply

The 4-channel high voltage supply used in this project (model number CAEN DT5534E) consists of two positive HV supply channels and two negative HV supply channels with an output range of up to 6 kV. To control the CAEN HV power supply, general control software for CAEN HV power supplies (GECO 2020) was used to achieve various operations such as powering it on/off and adjusting the specific voltage values for each channel.

2.1.5 Digital pulser processor

The digital pulse processor used in this project (model number DT5781) is upgraded from another DPP (model number DT5724), which was initially used as the data collection digitizer for the master project of F. Bohra [14] and L. Omar-Nazir [15].

Both digitizer models (DT5724 and DT5781) are four-channel, 14-bit systems provided by CAEN with a dimension of 154x50x164 mm3. The main difference between the two digitizers is the input impedance. The DT5781 model has an input impedance of 1 kΩ while the DT5724 model has an input impedance of 50 Ω. [18][19] Due to the large difference between the two input impedances, the decay times observed by the inspection software (MC2 and CoMPASS) contrast each other. The decay time for the DT5781 model is around 50 µs which is much longer than 20ns for the DT5724 model. More in-depth details about this hardware upgrade will be provided in later chapters.

To control the digital pulse processors, data acquisition laptops containing specific software are used. Both the MC2 software and CoMPASS software being used are developed by CAEN and have a list mode function that collects information on time and energy.

2.2 Data Acquisition software

The data acquisition software used in the system allows us to control various settings for the digitizer and view the spectrum in real-time. By switching the data acquisition software from MC2 to CoMPASS for this project, higher stability and a more user-friendly interface can be obtained.

2.2.1 MC2 Analyzer

The MC2 analyzer software developed by CAEN is designed for a digital multi-channel analyzer focusing on the management of data acquisition using the pulse height algorithm. The acquisition setup window for MC2 has an input signal section, a trigger section, and an energy filter section.[20] The figure below shows the interface of the acquisition setup window and the main screen for the MC2 analyzer. However, the MC2 is extremely unstable when collecting data.

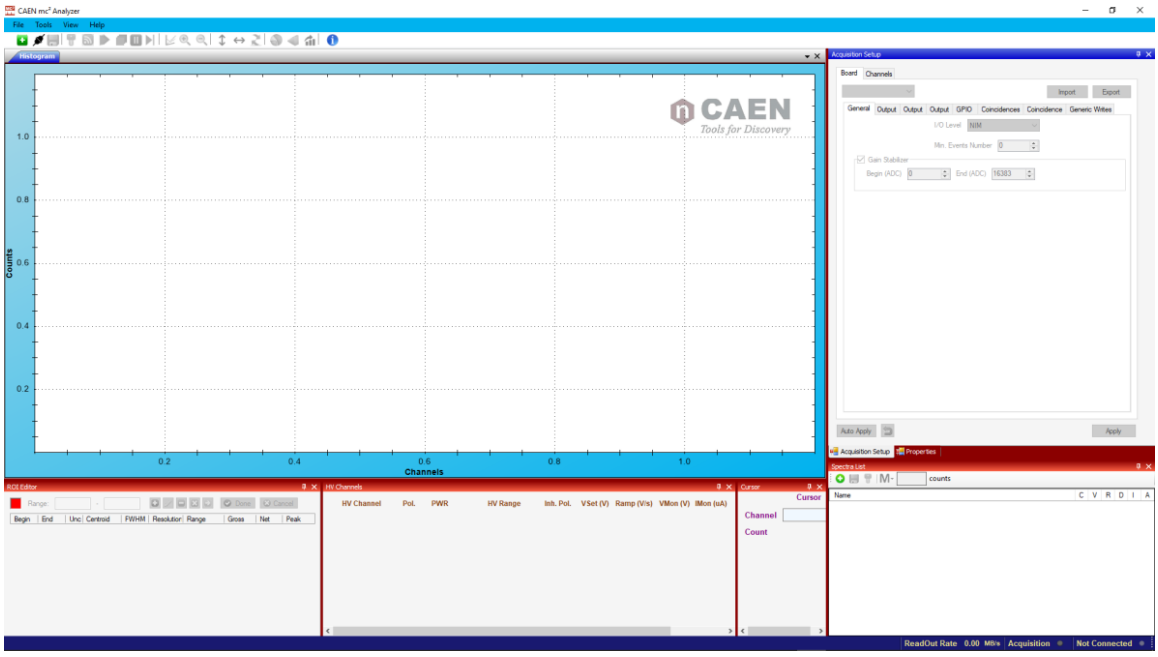

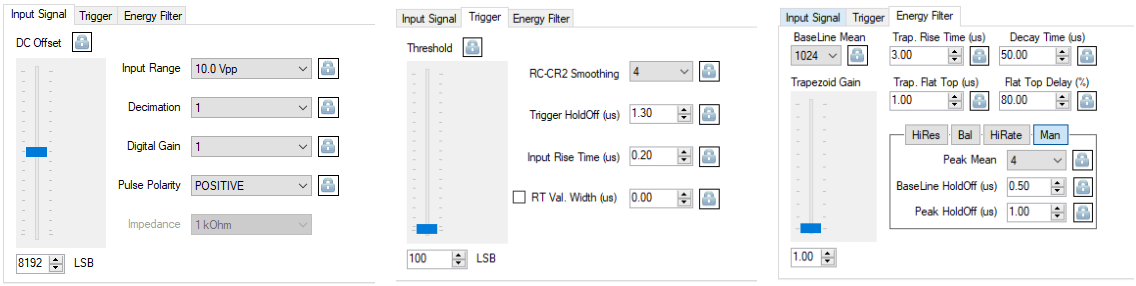

Figure 2.2 MC2 main screen view and data acquisition setting tabs

2.2.2 CoMPASS

The CoMPASS software is a new software from CAEN that can implement multi-parametric data acquisition for applications related to physics. The detectors can be connected directly to the digitizer's inputs, and the software acquires data on energy, timing, and PSD spectra. The highlight of the CoMPASS software is that it can manage the acquisition using all of the CAEN DPP algorithms, which include pulse height analysis (DPP-PHA) and pulse shape discrimination (DPP-PSD). [21] Compared to the MC2 software, CoMPASS has more versatility towards different types of digitizers and more functions such as the synchronization wizard, which allows configuration of the synchronization among multiple boards. The CoMPASS software is far from being thoroughly investigated, and many of its unused functions may still prove to be helpful for future research. A sample view of the CoMPASS interface is shown below.

Parameter	All
Enable	☐
Record length	20000 ns
Pre-trigger	2000 ns
Polarity	Positive
Ns baseline	256 samples
DC Offset	20.0 %
Input dynamic	1.0 Vpp

Parameter	All
Trap. rise time	2.000 µs
Trap. flat top	1.000 µs
Trap. pole zero	50.000 µs
Peaking time	80.0 %
Ns peak	1 samples
Peak holdoff	0.960 µs
Energy fine gain	1.000

Parameter	All
Threshold	100 lsb
Trigger holdoff	480 ns
Fast Discriminator smoothing	4 samples
Input rise time	100 ns

Figure 2.3 CoMPASS parameters for 1 Input signal, 2 Discriminator, 3 Trapezoid.

2.3 Changing of data acquisition software

As illustrated above, all previous studies used the MC2 analyzer as the primary data acquisition software. However, due to several reasons, the data acquisition software used for this project will be CoMPASS. This sub-section will explain the reasoning for changing the software to CoMPASS and the problems encountered during this process.

2.3.1 Motivation of changing software

The MC2 analyzer is a great software that meets our requirements for data acquisition. However, it has some crucial drawbacks. Firstly, the MC2 software is extremely unstable due to unknown reasons and is prone to crashing. Software crashes usually occur during the adjustment of parameters as well as at the end of the data acquisition process. When the crash happens, the software will stop responding, and the only way to fix this would be to restart the software. The constant software crash at the end of each measurement also decreases the experiment efficiency.

The second reason for changing the software is that CoMPASS has an auto-stop function after the setup data acquisition time. For most of the measurements in this project, a particular time of data acquisition is set. In the early stages, the vertical axis of the spectrum does not need to be converted to count rate; thus,

the spectrum can be more easily compared by just looking at counts overserved in a given time.

Finally, CoMPASS has more functions and parameters that can be adjusted, which allows us to set a higher upper limit for any future projects. Due to these reasons, following the CAEN staff's advice, the data acquisition software will be changed from MC2 analyzer to CoMPASS.

2.3.2 Similarities and differences between the two software

The MC2 Analyzer and CoMPASS are both developed by CAEN technology, meaning that they use CAEN digital approaches to build up the system.

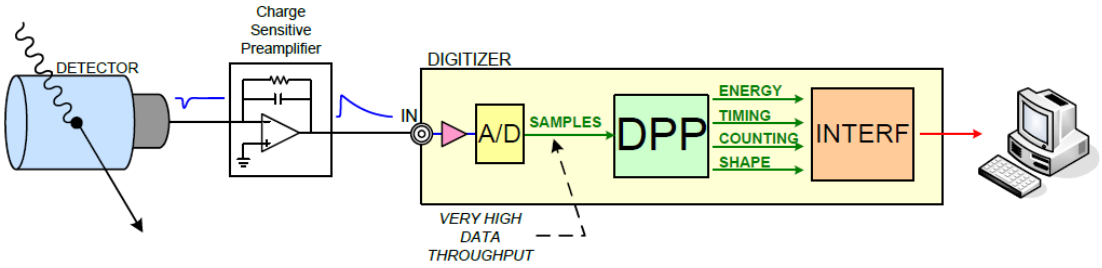

Figure 2.4 Block Diagram of a Digitizer -based Spectroscopy System [21]

The algorithm beyond the software and digitizers is DPP-PHA (Digital Pulser Processing for Pulser Height Analysis) based on the Jordanov trapezoidal filter. The trapezoidal filter can transform the typical exponential decay signal generated by a charge-sensitive preamplifier into a trapezoid with a flat top height proportional to the amplitude of the input pulse, which is usually the energy released by the particle in the detector.

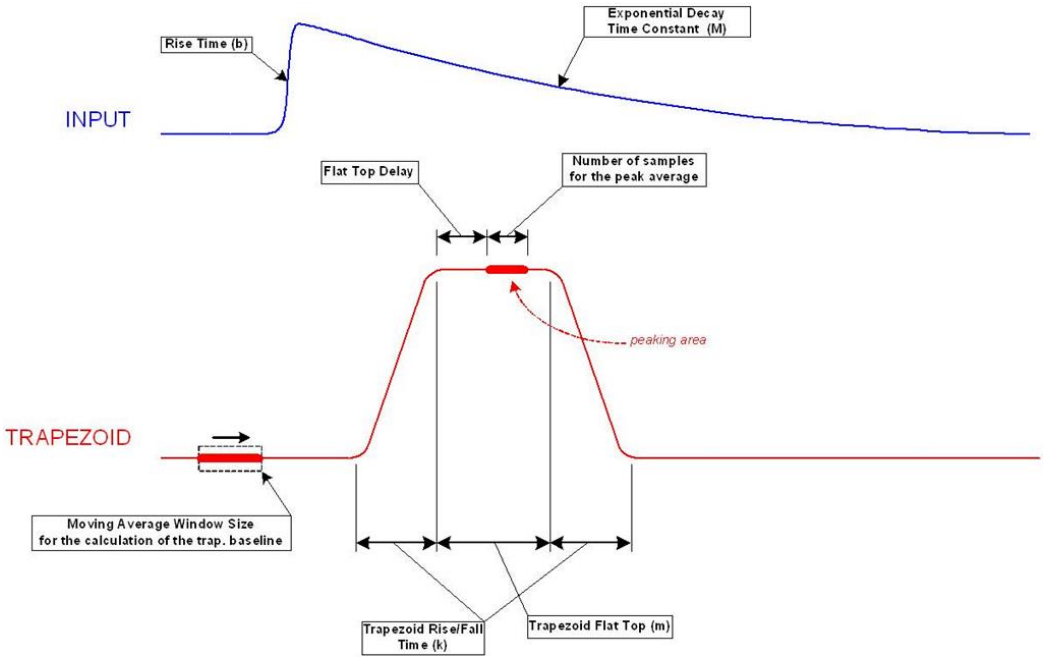

Figure 2.5 Pulse Height Analysis with Trapezoid Method. [21]

Although the two software has similar algorithms, the interface and the key parameters are quite different. The most critical parameters are the defining input signal, discriminator, and trapezoid filter. The following table shows critical parameters and their functions for both the MC2 and CoMPASS software.

Table 2.1 Important parameters in MC2 and CoMPASS [20,21]

Sub-section (Tab)	CoMPASS Name	MC2 Analyzer Name	Remark
Input	Polarity	Polarity	The polarity of the input signal (Positive/Negative)
	DC offset	DC offset	Baseline level of the input signal
	Input Dynamic	Input Range	Input dynamic range of the digitizer
	Threshold	Threshold	Threshold value to filter all the pulse
		RC-CR2 Smoothing	the RC-CR2 input signal second

Discriminator/ Trigger	Fast Discriminator Smoothing		derivative smoothing value
	Trigger holdoff	Trigger holdoff	Other trigger signals rejected within trigger holdoff time
	Input rise time	Input rise time	The rise time of RC-CR2 signal
Trapezoid/ Energy Filter	Trap. rise time	Trap. Rise Time	Rise time and the flat top of the trapezoid filter
	Trap. flat top	Trap. Flat Top Time	
	Trap. pole-zero	Decay Time	Make pole-zero adjustments to avoid overshoot and undershoot
	Energy fine gain	Trap Gain	Gain of signal's energy
	Peaking time	Flat Top Delay	Percentage of flat top duration

From the table above, we can see that all essential parameters have a one-to-one correspondence in CoMPASS and MC2, although the names for some of them may differ. CoMPASS is a more widely used software with more functions than MC2. Some of these function tabs that MC2 does not have include "Spectra", "Rejection", and "Energy Calibration". Since those tabs are not set in the project, they are not listed here for further illustration.

A critical parameter that is worth mentioning is the Energy fine gain/Trapezoid gain. In the MC2 analyzer, the gain has less restriction and could be set to over several thousand. However, in CoMPASS, the software only allows a value range of 0 to 10.

In almost all of our experiments, the Sr/Y 90 source is used to test the detector's performance. The height of the silicon detector's signal is low; therefore, events in the spectrum are usually clustered in the low channel region. If CoMPASS

modifies the energy fine gain parameter to over 10, the spectrum would move to a higher channel region. Since MC2 does not have an upper limit in the trap gain setting, the ideal spectrum should be achieved successfully.

In L. Omar-Nazir's thesis [15], the gain for the silicon detector was set to 140. Before the installation of CoMPASS, the DPP-PHA firmware in the digitizer was updated to fit the new software. After the MC2 firmware update, the gain setting was limited to a maximum of 10 for an unknown reason. The gain can still be set to above 10, but no signal would be shown. Besides adjusting the energy gain parameter in the software, changing the preamplifier's gain can also be used to increase the overall gain. However, the new preamplifier is still being shipped and cannot be solved until it arrives.

Overall, the CoMPASS software seems to have more outstanding performance when compared to the MC2 analyzer. Although both software utilizes the same DPP-PHA algorithm needed for the project, CoMPASS has higher stability and more functions to help future research.

Chapter 3 Method and System Setup

3.1 Pulse Processing Parameter optimization

Both the digital pulse processors and data acquisition software CoMPASS utilize DPP-PHA firmware that applies the trapezoid filter to the incoming signal. The parameters such as "input," "Discriminator," and "Trapezoid" need to be set up carefully to be able to see the ideal spectrum. [21,22] In this sub-section, the setup method for those parameters will be briefly introduced.

The input tab for CoMPASS includes three critical parameters that we need to pay attention to. The first one, polarity, should correspond to the pulse polarity of the detector and voltage polarity for the power supply. In this project, the silicon SBD detector's pulse signal is positive, while the plastic scintillator one should be negative, according to the detector's manual.

The DC offset value can be adjusted to move the input signal's baseline upwards or downwards, and the unit of the DC offset in the MC2 Analyzer is LSB (least significant digit) while the DC offset is expressed by percentages in CoMPASS. The DC offset should be adjusted so that the input signal's baseline covers its entire width to avoid saturation. Usually, the input signal is positive, and a relatively low DC offset is preferred.

The Dynamic range can be set in the "input dynamic" tab, which represents the full range of the signal in Voltages. The DT5724 digitizer has an input dynamic that is fixed to 2.25 V_{pp}. However, the input dynamic of the DT5781 can be adjusted to 0.3 $V_{pp,}$ 1 V_{pp}, 3 $V_{pp,}$ and 10 V_{pp}, which allows for another degree of freedom. [18,19] Most of these measurements use the DT5781 digitizer, so choosing the proper input dynamic is important. The input signals for the silicon detector usually have a small amplitude, so a common problem is not having enough gain and having all the events gathered in the lower channel in the

spectrum. In this case, a relatively smaller input dynamic causes the dynamic range to shrink and makes the signal's amplitude larger proportionally. Thus, the input dynamic would be set to 1 V_{pp} to increase all the events' channels. As for the plastic scintillator, the amplitude of the input signal is high enough, so the max input dynamic, 10 $V_{pp,}$ was chosen.

The Trigger and Timing filter (TTF) inside the digitizer is the filter that identifies the input pulses and generates a digital signal called the trigger. The trigger can then be used to identify the pulse by using the RC-CR2 filter. Parameters in the discrimination tab are adjusted to avoid noises and overshoot to be recognized as the events from the input signals. The discriminator tab consists of 4 parameters: "Threshold," "Trigger holdoff," "Fast discriminator smoothing," and "input rise time."

The first parameter to adjust is the "Fast discriminator smoothing" parameter. This parameter is defined as the number of samples used for the RC-CR2 signal formation. Increasing this parameter would potentially reduce the high-frequency noise and cause the drawback of making the signal slower and smaller. The smoothing factor was initially set to 16 for silicon and plastic scintillator detectors following the quick start guide. However, the noise level for the silicon detector was much higher than expected. Noises would be triggered as an event and shown in channel 0 in the spectrum. Due to this, the smoothing factor for the silicon detector was set to the maximum setting, which was 32.
After setting the smoothing factor, the following parameter is the "input rise time" parameter, which is the time that the RC-CR2 needs to reach its maximum value. This value is adjusted so that the RC-CR2 peak value equals the height of the input signal. Figure 3.1 below shows spectra with adjusted input rise time for both detectors.

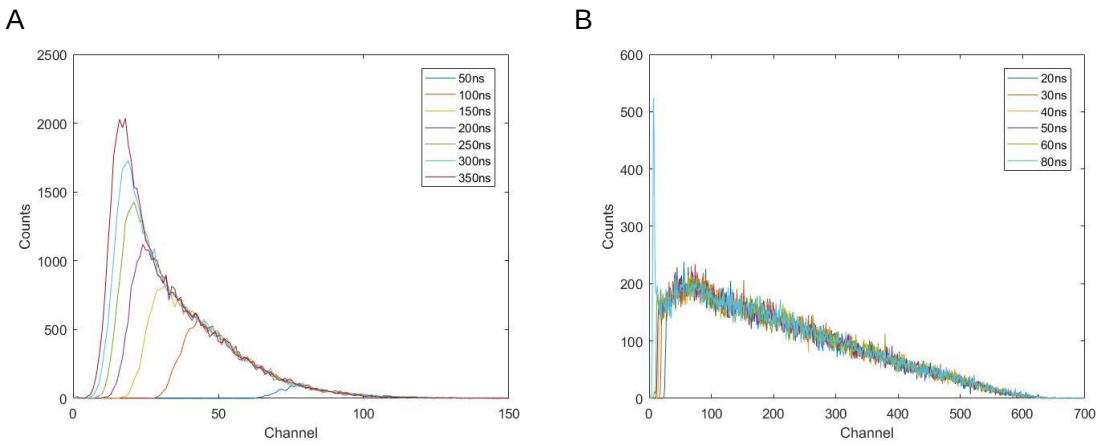

Figure 3.1 Sr/Y-90 spectrum with different input rise times for A) Silicon detector. B) Plastic Scintillator detector

"Trigger Holdoff" is the third parameter that can prevent data acquisition during the overshoot. The RC-CR2 signal for the plastic scintillator has an evident overshoot that can potentially be recognized as the second event with a smaller energy value. The holdoff value should be covering the RC-CR2 signal between the first zero crossing and all parts of the overshoot.

Finally, the "threshold" parameter is adjusted to filter all the noise signals. The RC-CR2 can also potentially contain a noise signal, and if the threshold is set too low, noises will be triggered, thus producing many events with nearly zero energy. However, if the threshold is set too high, some low-energy events would be lost. The experiment found that the spectrum's shape, especially the low energy part, is largely affected by the adjustment of the threshold. The lower the threshold, the more low energy events are detected and the higher the count rate. Some of the detected signals could be considered noise for unknown reasons. However, this "event loss" still happens when a relatively high threshold (15 LSB) is set. Although the plastic scintillator has a pretty low noise level, it still encounters this problem. Finally, both detectors' thresholds are set to 15 LSB to ensure all the noise is filtered even though it could potentially lose some events compared to a lower threshold. Figure 3.2 More tests about the event loss will be listed and discussed in the result section.

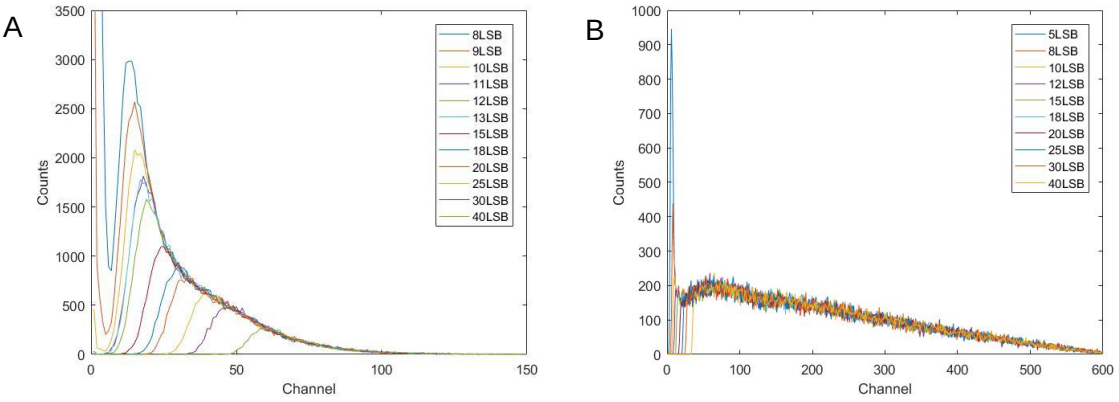

Figure 3.2 Sr/Y-90 spectrum with different input threshold for A) Silicon detector. B) Plastic Scintillator detector.

Parameters in the "trapezoid" tab control the energy filters. Various combinations of Trap. Rise time and Trap. Flat top is tested, and it has been determined that these parameters have minimal effect on the spectrum. The following figure 3.3 shows the effect of trapezoid parameters.

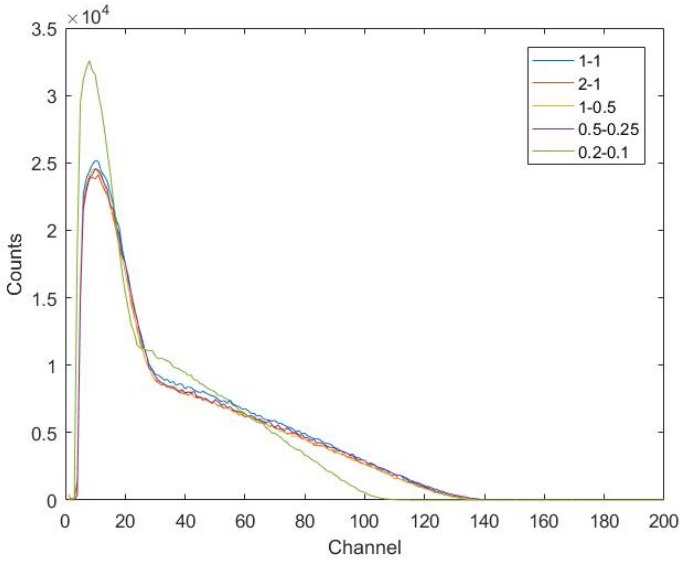

Figure 3.3 Sr/Y-90 spectrum with different trapezoid parameters (Trapezoid rise time - Trapezoid flat top) for plastic scintillator detector

Peaking time is adjusted so that the peaking position is in the flat top position. The energy fine gain can be regulated from 1 to 10 and adjusted to fit the energy range we are interested in after energy calibration. The gain limitations for CoMPASS are still a problem for silicon detectors, and a higher-gain preamp is currently being worked on to solve this.

The Trapezoid filter must return to the baseline at the end, which is 0 in this case. The "Trap. Pole zero" parameter is regulated to avoid the effects of undershooting or overshooting. The pole-zero adjustment can also decrease the effects of pile-up where the signal would not reach the baseline. To reduce the likelihood of pile-up events occurring, all sources used have a controllable count rate. Examples of undershooting and overshooting are shown below.

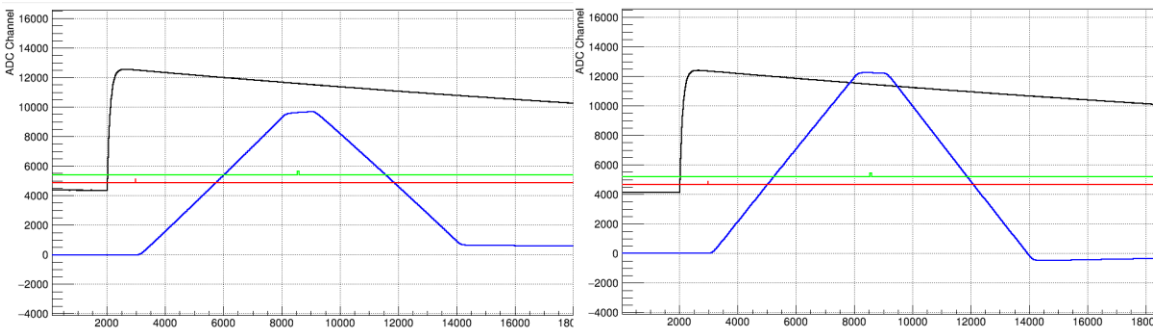

Figure 3.4 Two examples of undershooting(left) signal and overshooting(right) signal.[21][22]

3.1.1 Plastic scintillator parameters

The plastic scintillator is biased to -1000 V within 1024 ADC channels. Most of the parameters are optimized by following the CoMPASS user manual. Parameters not mentioned but listed below have a negligible effect on the spectrum; thus, the default values are used. Table 3.1 below summarizes the plastic scintillator detector's data acquisition parameters in three primary tabs.

Table 3.1 Plastic scintillator acquisition parameters

Tab	Parameter	Value	Parameter	Value

Input signal	Record Length	20000 ns	Ns baseline	256 sample
	Pre-trigger	2000 ns	DC offset	8.5%
	Polarity	Negative	Input Dynamic	10 Vpp
Discriminator	Threshold	15 lsb	Fast discriminator smoothing	16 samples
	Trigger Holdoff	600 ns	Input rise time	50 ns
Trapezoid	Trap. Rise time	0.2 µs	Ns peak	16 sample
	Trap. Flat top	0.1 µs	Peak holdoff	0.96 µs
	Trap. Pole zero	0.2 µs	Energy fine gain	4
	Peaking time	80%		

3.1.2 Silicon detector parameters

Silicon detectors are biased to +35 V with 1024 ADC channels. Parameters of the silicon detector are adjusted to the instructions of the CoMPASS user manual. Table 3.2 below summarizes the silicon detector's data acquisition parameters in three primary tabs.

Table 3.2 Silicon acquisition parameters

Tab	Parameter	Value	Parameter	Value
Input signal	Record Length	20000 ns	Ns baseline	256 samples
	Pre-trigger	2000 ns	DC offset	8.5%
	Polarity	Positive	Input Dynamic	1.0 Vpp
Discriminator	Threshold	15 lsb	Fast discriminator smoothing	32 samples
	Trigger Holdoff	150 ns	Input rise time	200 ns
Trapezoid	Trap. Rise time	2 µs	Ns peak	64 samples
	Trap. Flat top	1 µs	Peak holdoff	0.96 µs

	Trap. Pole zero	50 µs	Energy fine gain	10
	Peaking time	80%		

3.2 Coincidence set up

The diameter of the plastic scintillator (around 81.8 mm) is much larger than the silicon detector (around 19.36 mm), meaning that a holder is necessary for the silicon detector positioned in the middle of the plastic scintillator's detector face. A silicon SBD holder was 3D printed using PLA plastic with a thickness of 1.3 cm, an outer diameter of 7.6 cm, and an inner hole diameter of 1.3 cm.

The detector holder was used to house the silicon SBD during data collection and was mounted in front of the plastic scintillator. Silicon SBDs are sensitive to light; therefore, a 1.3 cm diameter, 50 µm thick Mylar sheet was taped to the detector holder to act as a window allowing it to shield the silicon SBD from light.

3.3 Modification of PMT signal.

At the start of the project, the DT 5724 digitizer was used as part of the beta spectrometer system and performed very well under different sources, which can be seen in the outputted spectrum. The wave inspector mode of the CoMPASS can show the shape of the input signal, RC-CR2 signal, and trapezoid filter. It has been noticed that the plastic scintillator's signal is extremely fast, with each detected event's input signal taking about 30-40 ns to decay back to the baseline. The frequency of the digitizer is 1 MHz; therefore, the time of each channel is 10 ns. In this case, the input signal only has a width of 3 to 4 channels.

A fast input signal is not an absolute drawback when an intense radiation field is expected. Under the extremely high count rate, a fast input signal with little time to decay can prevent the pile-up of events. However, the expected measuring

environment would not have a high enough count rate to make pile up a significant problem.

During data acquisition, both the time and energy information of the event should be focused on, with the decay time of the input signal balanced so that both values can be retrieved correctly. A faster signal gives better time-related information but also gives worse energy information. Attempting to slow down the signal, which will be introduced later, would improve the resolution and energy information but compromise the time information. In this project, the time information from both detectors is essential for the coincidence operation. The plastic scintillator's processing time is usually much faster than the silicon detector, meaning that it is acceptable to slow down the plastic scintillator's signal.

Generally, the decay time of the signal should depend on different circumstances. If the time information is more critical than the energy information, a fast signal would be preferred, such as the DT5724. However, energy resolution needs to be improved for the plastic scintillator; therefore, three different methods are used to slow down the input signal. These methods include adding a capacitor, changing the digital pulse processor, and adding a preamplifier for the plastic scintillator. In the following subsections, these three methods will be introduced.

3.3.1 Attempts of adding a capacitor to DT 5724

The first method of slowing down the input signal is to add a capacitor to the digitizer. Slowing down the input signal is equivalent to increasing the time constant. The decay time constant in an RC circuit is defined as:

$$\tau = R * C$$

Where R is the resistance and C is the capacitance.

The block diagram inside the digitizer is very complicated, but the input part can still be considered an RC circuit. Therefore, capacitance can still be approximately calculated from the estimated resistance and decay time constant. From the DT 5724 user manual, the input impedance of the digitizer is 50 Ω. [18] Several measurements have been conducted using an ohmmeter, and the measured resistance is 56.7±0.1 Ω. The decay time constant of the input signals from the plastic scintillator is hard to estimate directly. The figure below shows the waveform mode views from CoMPASS.

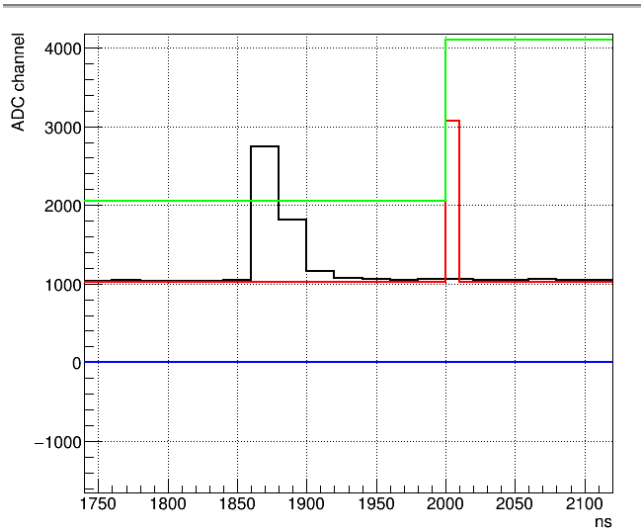

Figure 3.5 Typical input signal of the plastic scintillator (Black).

The input signal in the example shown above took around 100 ns to restore to the baseline. Decay over 99% of the pulse height is usually considered the restoration's completion; therefore, the estimated time constant is τ = 20 ns. The capacitance would be calculated by:

$$C = \frac{\tau}{R} = \frac{20ns}{56.7\Omega} = 3.53\ nF$$

Knowing the approximate input capacitance would allow us to figure out the capacitance we should add. Several different capacitors are chosen to increase the capacitance of the system.

Capacitors are added between the square bronze hole and hole labeled "Ground." Digitizer DT5724 is a four-channel digitizer, and only the capacitance of the channel connected to the plastic scintillator (CH1) was changed. The internal structure of the digitizer and capacitor placements are shown below in figure 3.6.

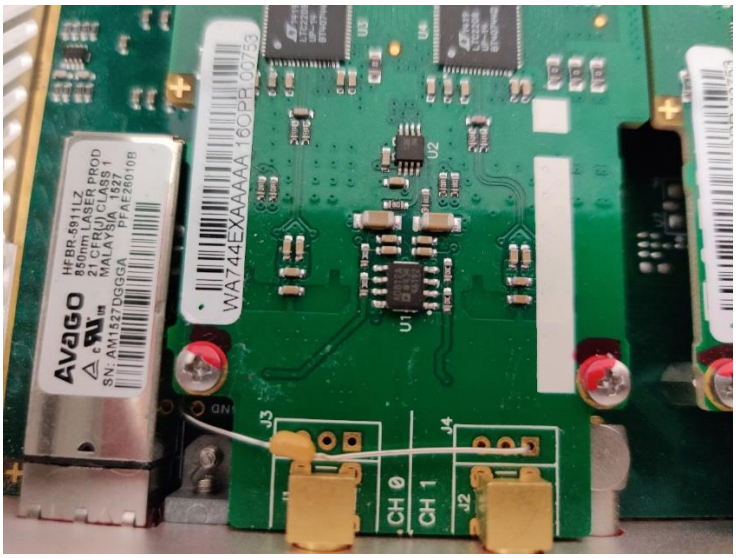

Figure 3.6 Internal change of digitizer DT 5724.

The addition of a capacitor changes the shape of the input signal to exponentially decaying oscillations, shown in figure 3.7 below.

A

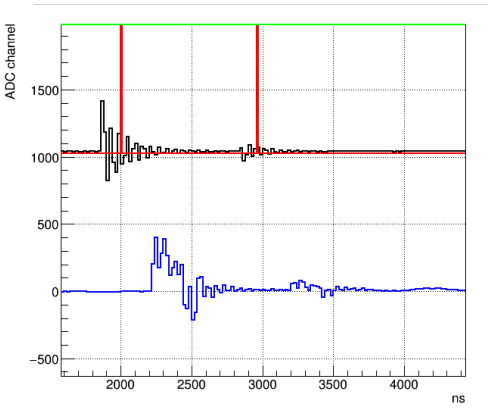

B

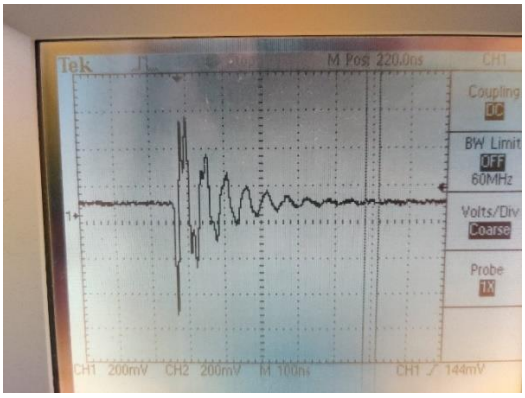

Figure 3.7 Shape of signals after adding 1 µf capacitor. A): Input (black) and trapezoid filter (Blue) in CoMPASS wave mode. B): Oscilloscope view of the input signal

The oscillation is caused by signal reflection. The reflection happens when the impedance of the source, cable, and load are unmatched. In this case, only part of the energy of the input signal is absorbed and transmitted. The rest of the energy is reflected in the opposite direction. Adding a capacitor would increase the input impedance of the digitizer. This may cause issues because the digitizer no longer has the same input impedance value as the cable. Therefore, the input signal coming from the cable would be reflected in the plastic scintillator detector. This unterminated reflection happens multiple times until the signal height decays to the baseline. The effect of this reflected signal and its oscillation cannot be correctly triggered for both the TTF and trapezoid filters.

A 50 Ω termination resistor is added in parallel to the detector to minimize the reflection. The resistance of the termination resistor should be equal to the characteristic impedance of the cable connecting the detector and digitizer. The resistance of the RG 58 cable used in this lab is 50 Ω. Therefore, a 50 Ω termination resistor is a reasonable choice.

After the termination, reflections disappeared as expected. However, the signal after the termination still had the initial problem to a greater degree. Figure 3.8 below shows the input signal after adding 1 µf capacitor.

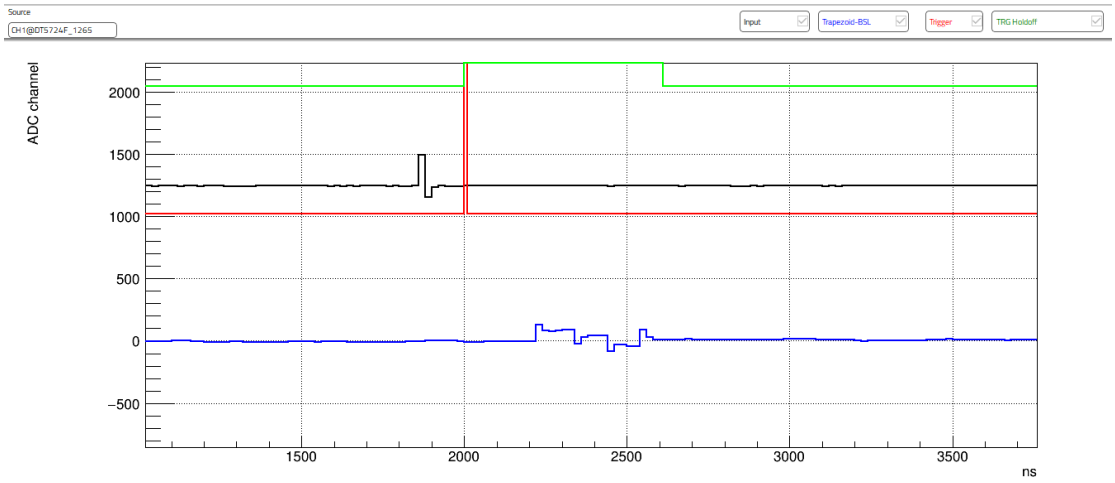

Figure 3.8 Shape of signals after adding 1 μf capacitor after termination

Compared to the figure above and figure 3.1, the decay constant between the terminated signal after adding a capacitor and the original input signal is similar. Capacitors with several different capacitances from 0.22 μf to 47 μf are tested. Theoretically, the new capacitance of the system and decay time would expand up to the order of tens of thousands depending on the capacitance added.

The figures above prove that adding a capacitor to the DT5724 digitizer could not achieve the goal of slowing down the signal due to an unknown problem. The attempts at adding capacitors provide valuable experience for solving problems. From the perspective of feasibility, changing the input impedance could still be a possible solution. A further study would be necessary to try to figure out the problem encountered in this method.

3.3.2 Addition of plastic scintillator preamplifier

The method of adding a capacitor did not accomplish the goal of slowing down the input signal. Therefore, another approach to increase the decay time constant should be considered.

As illustrated in chapter 2, the signal from the PMT is passed onto the digitizer without using a preamp. F. Bohra experimented by adding models of charge-sensitive preamplifiers between the digitizer and plastic scintillator detector. [14] The conclusion is that the signal would still be stable without any preamplifier. From the portability prospect of the system, fewer components would make measurement more convenient. Therefore, a plastic scintillator detector directly connects to the digitizer without a preamplifier.

The A1424 scintillation preamplifier, provided by CEAN, is a preamplifier that is designed explicitly for scintillator detectors. It can integrate both positive and negative input charge pulses coming from the PMT coupled to the Scintillator. It also provides a voltage signal in the ±4 V range on 50 Ohm termination with exponential decay (t= 50 μs) as Energy output (ENERGY).[23] The energy output of the preamplifier accomplished our goal of slowing down the input signal.

The sensitivity of the Charge Sensitive Preamplifier can be set via a 10-position rotary switch ranging from 0.8 to 10 mV/pC. The height of the resulting pulse is proportional to the integrated charge. The sensitivity would be the slope of the pulse height vs. the integrated charge function and can be adjusted as a parameter that has a similar function with the energy fine gain. Figures 3.9 below show the form of the input signal with a preamplifier and the experiment showing the spectra with different sensitivities.

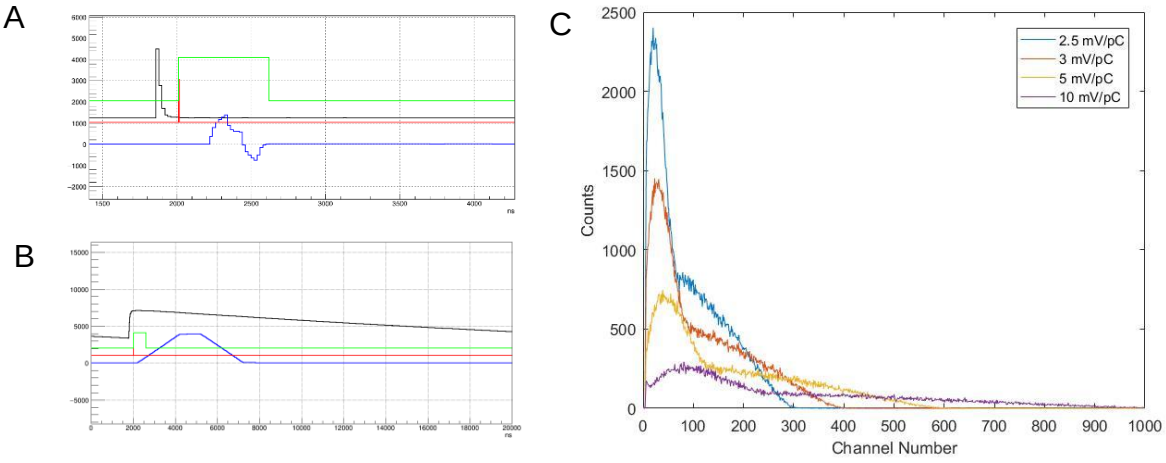

Figure 3.9 A) Shape of the input signal in DT 5724 without preamplifier(Black). B) Shape of the input signal in DT 5724 with preamplifier (Black). C) Sr/Y-90 spectrum with various preamplifier sensitivity

By adding a scintillation preamplifier, it is evident that the decay time is significantly increased. With the longer decay time, the shape of the trapezoid filter improved due to more digitized points. Although the input signals are slowed down, the additional component of the system is still unpreferred. The optimal solution is to modify only the digitizer.

3.3.3 Upgrade of Digital pulse processor

The scintillation preamplifier gives a solid solution to modify the PMT signal. However, another method that keeps the simplicity of the system would still be preferred. All the above approaches are based on the DT 5724 digitizer, which is the model used by F. Bohra and L. Omar-Nazir. As the decay time problem arises from the limitation of the digitizer, it would be reasonable to change the digitizer and slow down the PMT signal.

The DT5781 digitizer provided by CAEN is a superior solution for this problem. As introduced in section 2.1.5, two digitizers are pretty similar in various specifications as well as the algorithm of digital pulse processing. The hardware upgrade from DT5724 to DT 5781 is due to the contrasting input impedance differences. The DT 5781 results in a longer decay time of the PMT input signal since the digitizer has a more significant input impedance of 1 kΩ.

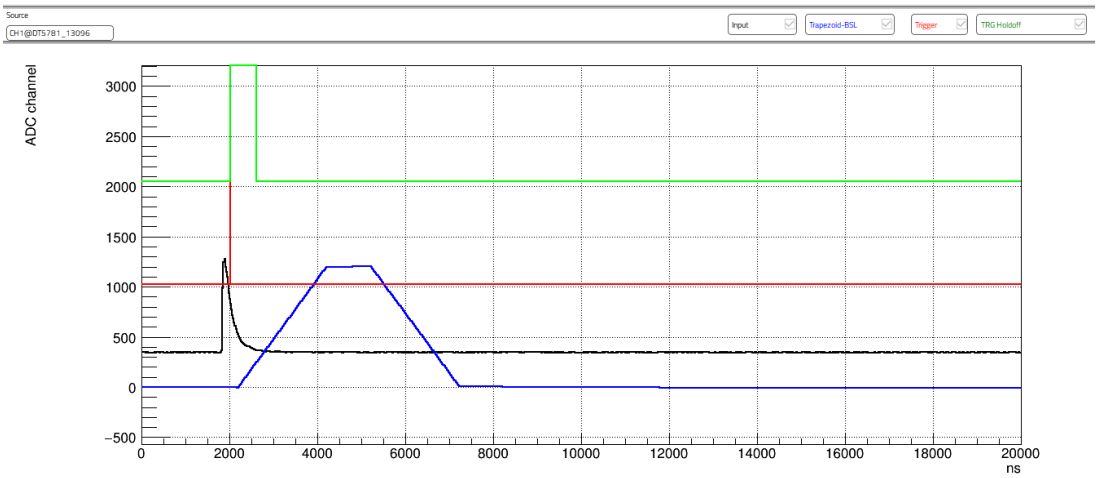

Figure 3.10 Shape of the sample input signal in DT 5781 (black).

An increased decay time of approximately 0.3 µs is observed from the figure above. The decay time increase due to changing the digitizer is much less than the increase due to adding a scintillation preamplifier (approximately 50 µs). However, as the input signal has more digitized points than the original digitizer, changing the digitizer would be a solid solution for slowing down the signal.

Chapter 4 Monte Carlo Simulation

MCNP (Monte Carlo N-Particle transportation code) is a powerful tool that can simulate various detector systems and sources. The MCNP6 was used to simulate the Silicon and Plastic scintillator detector system's response under various beta and gamma sources in this project. By generating millions of particles, it provided the theoretical spectrum of many certain experimental cases. Data from an unknown field can be deconvoluted to obtain the fluence rate spectrum from the known responses of the system. Coincidence spectrum simulation did not include in this chapter. The investigation of PTRAC function in MCNP is required in the future to complete the coincidence spectrum simulation.

4.1 Modeling of the beta spectroscopy system

4.1.1 Detector constructions

To simulate the performance of the beta spectroscopy system, indicating the construction of the detector's geometry defined by surface card and cell card would be the first step. Modeling the plastic scintillator detector was based on the schematics of detectors, shown in figure 4.1 below.

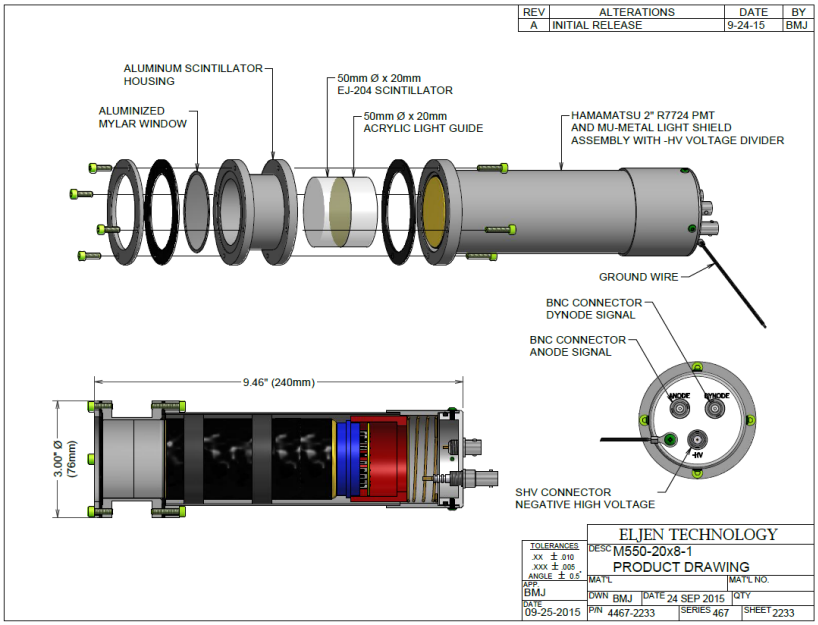

Figure 4.1 The product drawing of the plastic scintillator housing provided by Eljen Technology.

From the near to the far side of the source, simulated structures include Source, Source mylar, mylar, 3D printed plastic holder, Silicon semiconductor detector, Aluminum case, scintillator, PMT, and light guide. The coin source of Sr/Y-90 was located at the front part of the detector system, thus preventing particles from hitting the detector from the backside. The silicon detector was mounted inside the 3D-printed plastic holder in front of the detector face of the plastic scintillator. For the plastic scintillator detector, the interaction part is the Scintillator part of ej204. Particles can penetrate the front side structure and be scattered by the material at the backside structure, and change the direction. Thus, other parts at the backside of the detector, including PMT and light guide, are also included. Due to that, in some extreme cases, the particle can hit the detector from a large angle to the incident direction with multiple times of scatter. It is essential to include the most detailed structure for the simulation. The structure view from Visual Editor is shown below in figure 4.2.

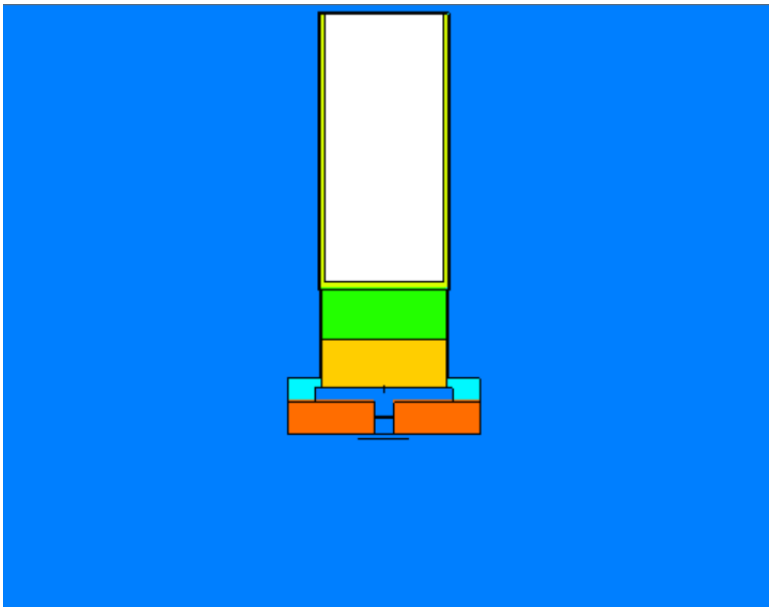

Figure 4.2 MCNP configuration of the beta spectroscopy system in cross-section view visualized by VISED.

4.1.2 Source cards for the simulation

The target of the system would be identifying the beta spectrum from the beta/gamma mixed field. The mono-energy beta source was simulated firstly to test the performance of the modeling of the beta spectroscopy system. The simulation of the Sr/Y-90 disk source is the central part of this section, as it is the major beta emitter used in the lab. Besides the Sr/Y-90 disk source, gamma emitter Cs-137 was also simulated at the same source position.

Disk source with various diameters at the front of the system was defined in the source card of the input file. Active elements are distributed on a very thin layer underneath the aluminum mylar. More specific source geometries for Sr/Y-90 and Cs-137 sources are shown below in Figure 4.3. [24,25]

A

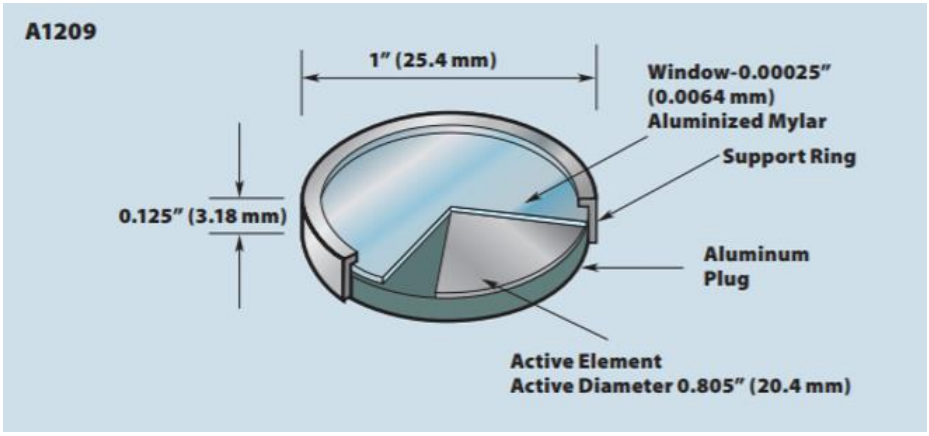

B

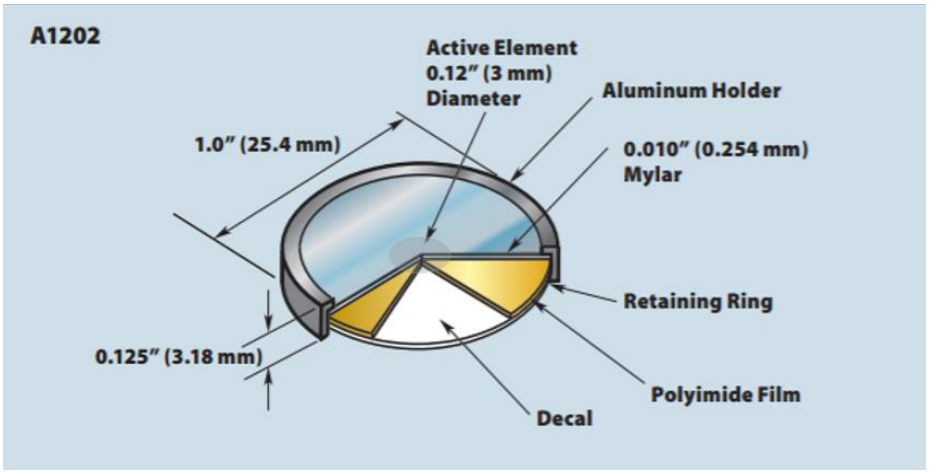

Figure 4.3 Geometries of disk sources used in the experiment. A) Sr/Y-90 B) Cs-137

Besides the source geometry, beta energy is also essential to figure out. Both Sr-90 and Y-90 emit beta particles with a specific range of energies. Source information card includes 15 checkpoints with corresponding energy. Source energy for strontium and yttrium is shown below as Figure 4.4, retrieved from RADAR (the RAdiation Dose Assessment Resource) [26]. The simulations of Sr-90 and Y-90 were executed independently.

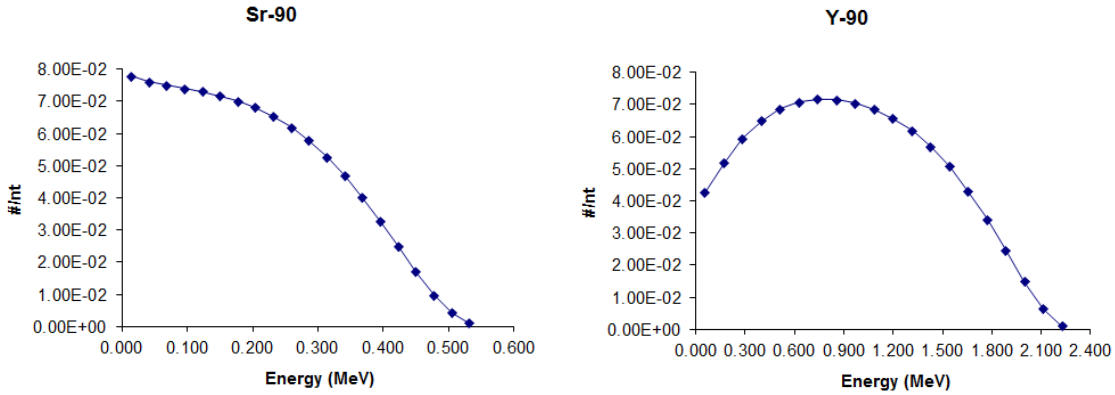

Figure 4.4 Energy spectrum of beta particles emitted from Sr-90 and Y-90 sources [26]

4.1.3 Material card and tallies

The model consists of 9 materials, including aluminum, air, yttrium, silicon, scintillator, acrylic, glass boron, PLA, and mylar. The composition of organic matters can be found in the PNNL-15870 report. [27] The spectrum of each simulation and energy deposition is the critical information interested. Therefore, F8 and *F8 tally were used for the input file. The build-in command gaussian energy broadening (geb) applying a Gaussian probability distribution to the deposited energy for every particle was included in the MCNP input file.

4.2 Simulation result

4.2.1 Mono-energetic beta particles

The first source applied for the simulation was mono-energetic beta particles for a 1.02 cm radius disk source. The energy range of particles varies from 500 keV to 3 MeV with an interval of 500 MeV. Total number of 1×10^6 beta particles were simulated at each energy. The absolute detector efficiency was calculated from the summation of normalized count acquired from the result of the F8 tally. With the increase of beta energy, both absolute efficiency for silicon SBD and

plastic scintillator steadily increase, as shown in Figure 4.5 below. Despite the increasing trend, the absolute efficiencies are still relatively low, 5.97% for 6.20% for silicon and plastic scintillator, respectively.

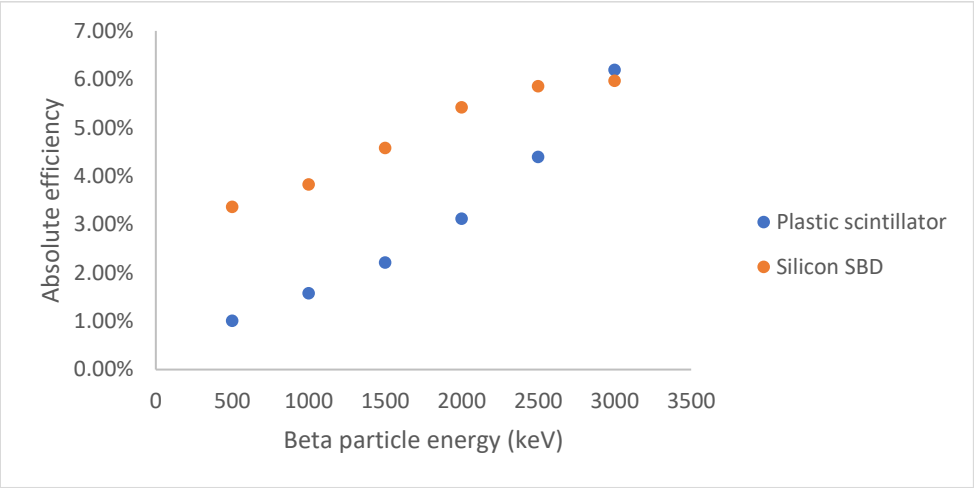

Figure 4.5 Absolute efficiency for plastic scintillator and silicon SBD under mono-energetic disk beta source.

The spectra of mono-energetic beta particles are shown below in figure 4.6. For the plastic scintillator, the beta energy peak moves towards a high energy region with the increase of incident beta energy. At the same time, more particles would spread to lower energy range, and peak height shirks except in the case of 3 MeV incident energy. The silicon SBD can only fully stop beta particles of approximately 130-140 keV. Therefore, for our simulated energies over 500 keV, only a fraction of the incoming particle energy is deposited in the silicon SBD. The spectrum shape of the silicon is stable, indicating that the energy loss of beta particles would be stable no matter the beta energy. More interaction happens with the increase of beta energies, given that the peak height of the spectrum keeps increasing.

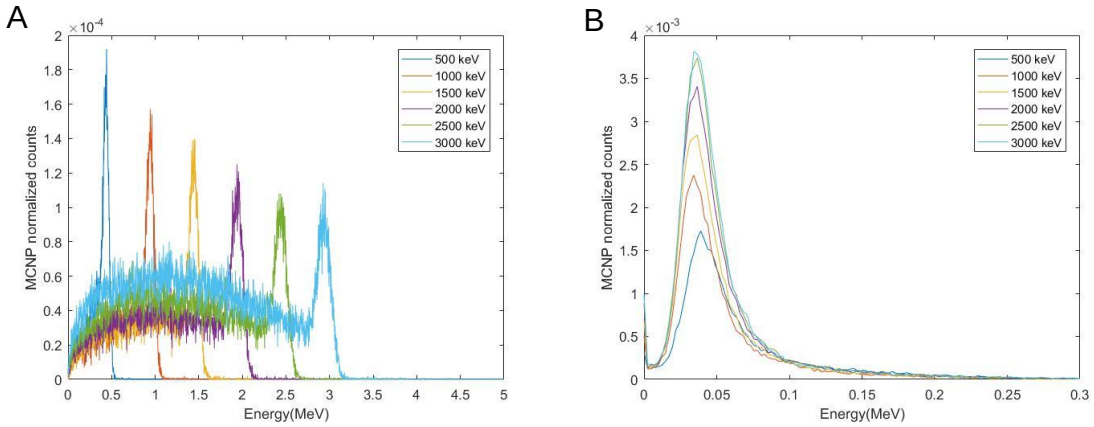

Figure 4.6 Pulse height spectrum of mono-energetic disk beta source simulations for A) Plastic scintillator B) Silicon SBD

4.2.2 Sr/Y-90 disk source

The beta emitter Sr/Y-90 disk source was simulated to test the performance of the beta spectroscopy system. The absolute efficiency and energy loss for both detectors are shown in table 4.1 below. The energy losses for silicon SBD are relatively close between strontium and yttrium. In the meantime, the strontium source with lower energy would cause much lower absolute efficiency and energy loss for the plastic scintillator.

Table 4.1 Simulated absolute efficiency and energy loss for beta source Sr/Y-90

Beta source	Detector	Absolute efficiency	Energy loss
Sr-90	Plastic scintillator	0.294±0.005%	0.579± 0.002 keV
	Silicon	2.548±0.015 %	2.268±0.016 keV
Y-90	Plastic scintillator	1.47±0.008%	11.11±0.11 keV
	Silicon	3.920±0.005%	2.342±0.016 keV

The spectrum of Sr/Y-90 is figured by summing the pulse height of two radionuclides. Simulated spectra were also compared with the calibrated energy spectrum measured in the lab at Figures 4.7c and 4.7d. A noticeable shape

difference exists between the lab measurement and simulation spectrum for the plastic scintillator. Shaping parameters, in this case, could affect the lab measurement spectrum to a large extent. For instance, a higher threshold prevents the event collected at low energy channels. Another shape difference would be simulated spectrum decay faster than measured spectrum. In the meantime, the turning point between the strontium and yttrium branch is challenging to find. A reasonable guess for this difference is that severe event loss may happen in the strontium branch due to the limitation of data acquisition software or inaccurate simulation modeling. As for the silicon spectrum, although the shape difference between simulation and experiment is much less, a better energy calibration could help to improve the spectrum.

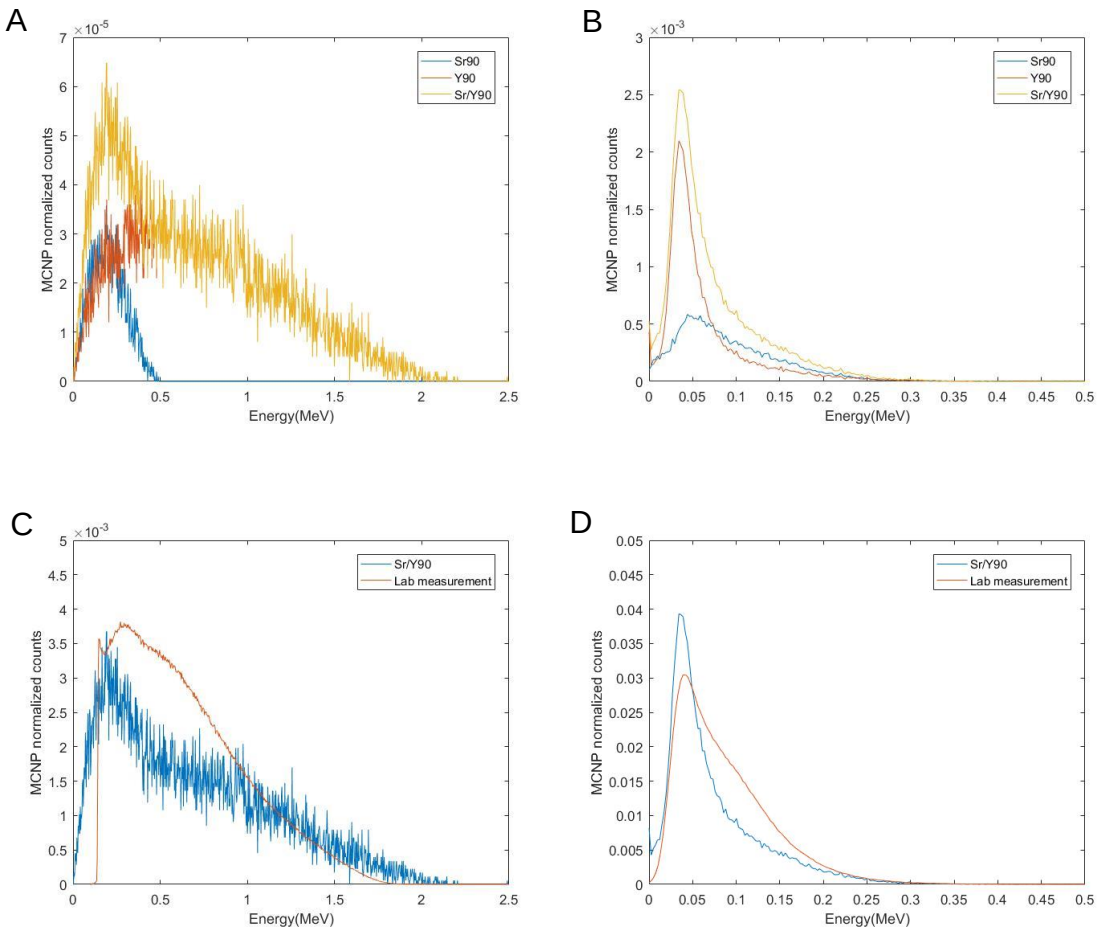

Figure 4.7 Sr/Y disk source simulation result. Simulation spectrum for A) Plastic scintillator B) Silicon SBD. Comparison between simulated and measured spectrum for C) Plastic scintillator D) Silicon SBD

4.2.3 Cs-137 disk source

The simulation of the Cs-137 disk source, which was the gamma source used in the experiment, is necessary to test the system's performance under high count rate gamma fields. The absolute efficiencies of the simulation are 37.45±0.05% and 9.52±0.03% for plastic scintillator and silicon SBD, respectively, which are much higher than the case of Sr/Y-90. The simulated plastic scintillator spectrum was compared with the measured spectrum in the lab, shown in figure 4.8 below. Although the low energy region for the measured spectrum was missing due to the shaping parameter and energy calibration error, the Compton maxima part of the Cs-137 spectrum overlapped.

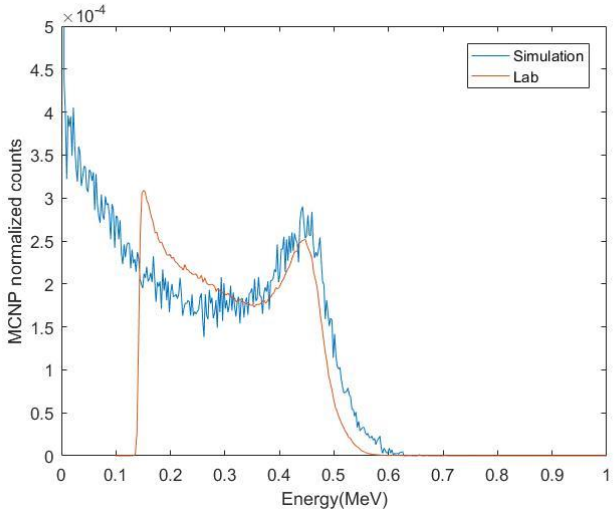

Figure 4.8 Comparison between simulated and measured plastic scintillator spectrum for Cs-137 source.

Chapter 5 Experiment result

5.1 Energy calibration

Calibration is an impotent step of the data analysis that converts the unit of the spectrum's horizontal axis from channel to energy. The energy range focused in this project is 700 keV to 3 MeV; therefore, the system's gain should be appropriately adjusted. If the corresponding energy of the maximum channel (channel 1024 in this project) is far higher than the upper limit of the focused energy range, the energy represented by each channel will also increase, which is unpreferred. This section will introduce the calibration method and the calibration equation for the plastic scintillator and silicon detector.

5.1.1 Plastic scintillator calibration

The calibration method using Compton Edge (CE) for plastic scintillator is conducted by F. Bohra.[14] Compton edge is defined as the maximum energy transfer to the recoil electron. This extreme case is usually considered as a head-on collision in which scattering angle θ=π. The Compton edge of Cs-137 and Co-60 is used in energy calibration, calculated by the equations below.

$$CE = E_\gamma - E_\gamma' \quad Eqn\ 5.1$$

Where the energy of the scattered photon E_γ' is given by:

$$E_\gamma' = \frac{E_\gamma}{1 + \frac{E_\gamma}{m_e c^2}(1 - cos\theta)} \quad Eqn\ 5.2$$

Plug scattering angle θ=π and rewrite Eqn 5.1 above:

$$CE = \frac{2E_\gamma^2}{m_e c^2 + 2E_\gamma} \quad Eqn\ 5.3$$

The CE for Cs-137 and Co-60 (1173 keV incident photon) is calculated to be 478 keV and 963 keV, respectively. Compton maxima (CM) is the Compton edge after the detector energy broadening effect. After applying the energy resolution effect, the ratio R was found between CM and CE at the simulated deposited energy spectrum.

Lab spectrum of Co-60 and Cs-137 were collected in the modified setting with new software and parameters. The channel number of the CE would be figured out using the ratio R indicated by F. Bohra. [14]

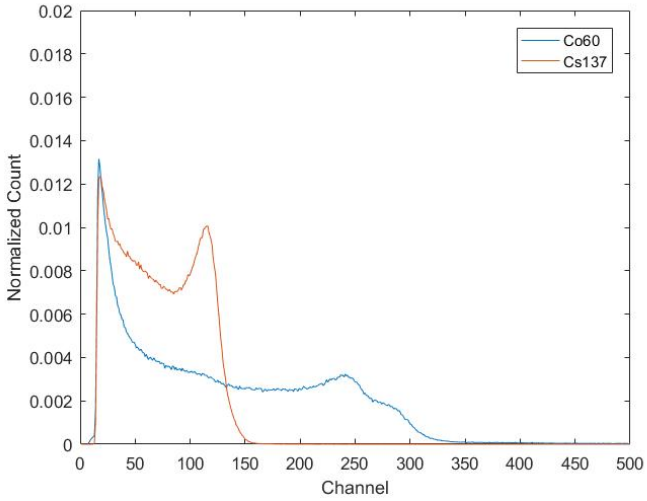

Figure 5.1 Calibration spectrum of Co-60 and Cs-137.

Source	CE Energy (keV)	Ratio	CM Counts	CM Channel	CE Counts	CE Channel
Co-60	478	0.58	13085	116	7589	126
Cs-137	963	0.52	4128	237	2146	286

Table 5.1 Determination of the acquired spectrum channel number that corresponds to the Compton Edge energy value for the Co-60 and Cs-137

The energy of each channel was also estimated by the curve fitting tool of the Sr/Y-90 spectrum. Sr/Y-90 is the main beta emitter used in the lab that has two branches, Sr-90 and its daughter radionuclide Y-90. Both branches have corresponding maximum energies, which are 546 keV and 2284 keV,

respectively. The curve fitting tool in MATLAB was used to figure out the channel corresponding to the maximum energy of the Sr-90 and Y-90.

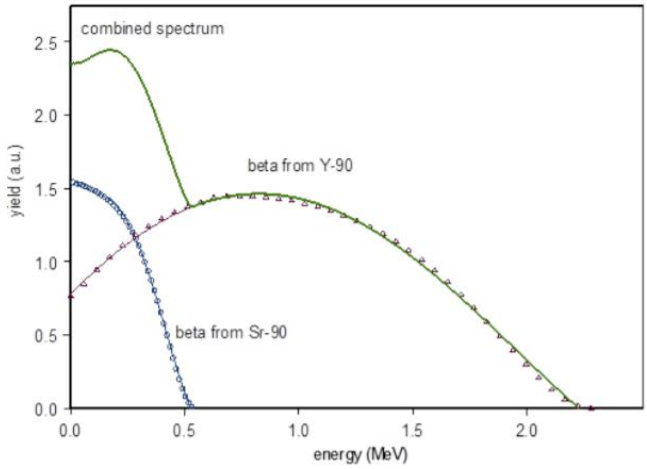

Figure 5.2 Sr-90 and Y-90 branch in the spectrum of beta emitter Sr/Y-90. [28]

The estimation of the two maximum beta energies from MATLAB would still be inaccurate when considering the fluctuation of the spectrum's curve. Therefore, although this calibration method conducts a better calibration equation, especially in low energy channels, the calibration data from the Compton edge method was used in all the further data analyses.

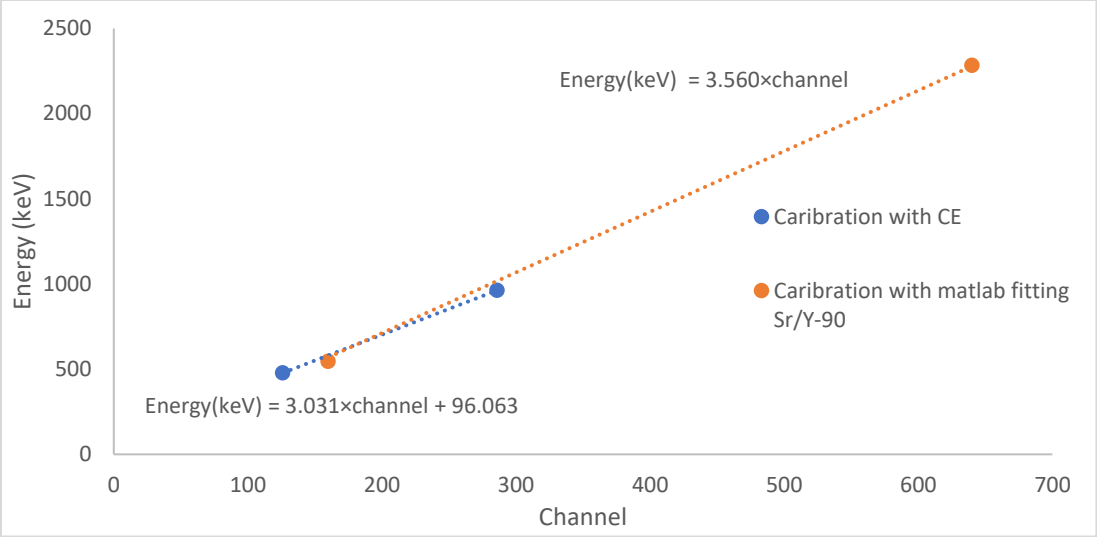

*Figure 5. 3 Energy calibration curve for **the** plastic scintillator with different methods.*

The calibration equation for the plastic scintillator detector was determined to be Energy(keV) = 3.031×channel + 96.063, with the dynamic range being 3.2 MeV. The non-zero intercept of the equation indicates that energy corresponding to lower channels would be inaccurate.

5.1.2 Silicon detector calibration

Alpha particles from Am-241 and Cm-244 were used in Silicon SBD calibration. Energies carried by alpha particles emitted from Am-241 and Cm-244 are 5.49 MeV and 5.81 MeV, respectively. Although sources were placed as close as possible to the detector surface, the energy loss in the air still needs to be considered when processing energy calibration due to the shorter range of alpha particles.

The energy loss of alpha particles was calculated by SRIM. SRIM (the Stopping and Range of Ions in Matter) is a powerful software package that could quickly generate the table of the mass stopping power for any ion at any energy in any elemental target. The linear stopping power S is defined as:

$$S = -\frac{dE}{dx} \quad Eqn\ 5.4$$

Where E is the energy of charged particles, x is the distance traveled in the path.

When the mass stopping power $\frac{\rho}{S(E)}$ is given by SRIM, the length of a particle with initial energy E_i traversing through a material ending up with final energy E_f can be calculated by

$$L = \frac{1}{\rho}\int_{E_i}^{E_f} \frac{\rho}{S(E)}\, dE \quad Eqn\ 5.5$$

Where ρ is the density [mg/cm^3] of the material.

The stopping power table given by SRIM was converted to the stopping power equation in the air by linear interpolation. Plugging the fitted stopping power equation, initial energy, and the air density to equation 5.5 above, both energy loss and calibration energy can be calculated. The range of alpha particles with 5.5 MeV is approximately 27-30 µm; therefore, the full energy deposition is considered in this situation. The result is summarized in table 5.2 below.

Table 5.2 Calculated energy loss of alpha particles by SRIM

Source	Incident Energy (MeV)	Energy loss (MeV)	Calibration energy (MeV)	Stopping power at E_{max} (mg/cm^2)
Am-241	5.49	0.3235	5.1665	0.7211
Cm-244	5.81	0.3324	5.4776	0.6928

The beta events collected by the silicon detector have lower energy; therefore, the gain was set to be as large as possible. The alpha energy is beyond the dynamic range of the spectrum, so a pulser was used to convert energies of alpha peaks from the lower gain's spectrum to the optimal setting.

Table 5.3 Calibration of the silicon detector with pulser

Source	Calibration energy (MeV)	Channel of alpha peak (lower gain)	Pulser amplitude (lower gain) (V)	Pulser amplitude (optimal) at same channel (V)	Energy (optimal) (MeV)
Am-241	5.167	607	0.347	0.107	1.590
Cm-244	5.478	644	0.369	0.114	1.696

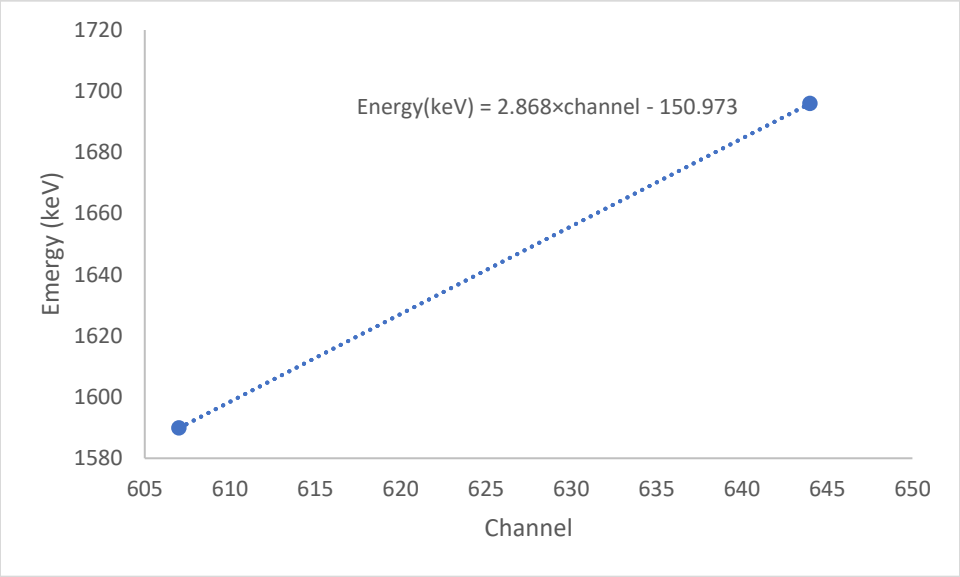

Figure 5.4 Energy calibration curve for silicon detector.

The calibration equation for the silicon detector was determined to be Energy(keV) = 2.868×channel - 150.973, with the dynamic range of this calibration being 2.79 MeV. Same as the calibration equation of the plastic scintillator, the non-zero intercept led to inaccurate energy of the lower channel. Compared to plastic scintillators, more events collected by silicon detector gathered in low energy range; therefore, the uncertainty would more severely affect the spectrum.

5.2 Benchmark test of different set-up

As introduced in section 3.3, both adding plastic scintillator preamplifier and changing digitizer were proved to be solid solutions for the too-fast signal for plastic scintillator. The benchmark test would be essential to test the

performance of all four scenarios: DT 5724 or DT5781, with or without a preamp. The spectra of Sr/Y-90 were collected under the same shaping parameters. The only changing parameter was energy fine gain, which was adjusted to reach the optimal dynamic range.

Table 5.4 Number of counts collected by the system of four set-ups with given time.

Set up	Input	Pile up	Saturation	Output	Real time(s)	Dead time (%)
DT5724	1124007	9027	27	1107371	100	1.48
DT5724+Preamp	1078187	7403	20	1063975	100	1.32
DT5781	1142258	8937	34	1125530	100	1.46
DT5781+Preamp	1105223	8021	660	1089394	100	1.37

Input count consisting of output count, pile up counts, and saturation counts is the total number of counts imported from the detector to the software. Output count is the number of counts shown in the spectrum and result txt file. The table above indicates that the input count rate for four different settings is pretty similar, which is $(1.11 \pm 0.03) \times 10^4$ counts per second. The percentage of the range is 2.9%. The source of this difference could be from the minor source movement when changing the setting and the low energy event fluctuation. Pile-up and saturation event ratios are relatively low from the table.

Spectra of four different set-ups are shown in figure 5.5 below. DT5724 without preamplifier could not reach the ideal channel with the highest gain. Therefore, the low-energy region has a higher count rate. In the meantime, all the other three settings give spectrum with a similar shape, especially in the Y-90 branch. In the spectrum of DT5781 with a preamplifier, the number of the bad event (gathered in channel 0) is relatively high, which leads to a higher number of saturation counts. This error would come from the setting of the preamplifier and CoMPASS software.

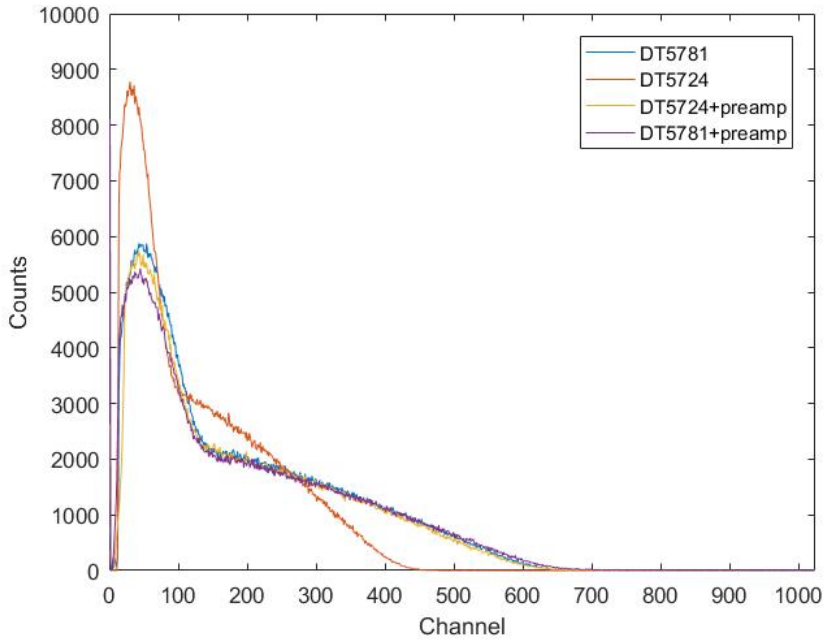

Figure 5.5 Sr/Y-90 spectrum of four set-ups with given time

Another phenomenon that is worth noting would be the low channel event loss. When the signal's amplitude is relatively small and close to the threshold, it is noticed that some events will be filtered out. The event loss starts in some specific channel that is dependent on threshold and hardware. The spectrum lower than that channel could not be fully trusted. This lowest trustable channel was figured out by the generating signals with different amplitude by pulser connected to the digitizer.

Table 5.5 Lowest channel and corresponding trustable of four set-ups figured by pulser.

Setting	Dynamic range (keV)	Trustable channel	Trustable energy (keV)
DT5724	5065.3	94	486.6
DT5724+Preamp	3333.8	34	151.9
DT5781	3651.6	43	142.4
DT5781+Preamp	3432.0	25	119.0

The spectrum of digitizer 5724 without preamplifier has the highest trustable energy of 486.6 keV, which means the event in the vast range cannot be fully trusted. The maximum energy (in channel 1024) is 5.07 MeV, also far more extensive than our expectation of 3 MeV. The other 3 case shows similar max energy and trustable energy in the acceptable range.

Figure 5.5 and Table 5.5 prove that both the method of adding preamplifier to plastic scintillator or changing new digitizer improve the performance of original setting in the aspect of maximum gain and lowest trustable channel. Although the two methods show similar spectrum and trustable energy, the changing digitizer was chosen as the final solution to the slow signal problem due to portability.

5.3 Coincidence window determination

The coincidence time window is a time constant that needs to be carefully determined. If the time between a silicon event and a plastic scintillator event is less than a coincidence time window, it is considered a coincidence event. For any coincidence event, silicon SBD is always the detector that firstly interacted with, as silicon SBD was placed in front of the plastic scintillator. In such a case, the time stamp of the silicon detector must be smaller than the plastic scintillator detector. The determined coincidence time window of 0.2 μs from Laila's master thesis proves that the silicon signal arrives digitizer earlier than the signal of the plastic scintillator. However, the coincidence time window determined from the list data collected by CoMPASS and updated hardware disapprove of the fact. The signal from the plastic scintillator arrives earlier than the silicon signal. The processing time difference would probably be the reason leading to this unusual phenomenon. The signal for plastic scintillator is much faster than silicon SBD, and it is possible to arrive at digitizer faster than event signal from silicon SBD.

The determination of the coincidence time window starts with plotting the histogram of the time difference between a silicon event and the closest plastic scintillator event by MATLAB, shown in figure 5.6. The time difference is binned

in the range of 0 to 1 μs and 0 to 100 μs. The majority of events from the silicon detector occurred within 1 μs after events from the plastic scintillator, shown in figure 5.6A. Among those events with a time difference of less than 1 μs, most of the events take place within 0.3 μs, as displayed in Figure 5.6B.

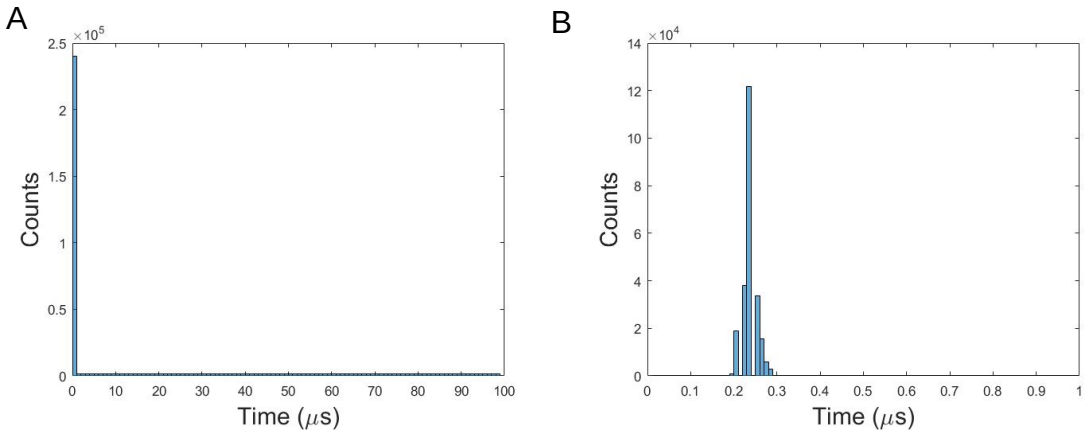

Figure 5.6 Time between events for Sr/Y-90 A) Binned from 0 to 100 μs B) Binned from 0 to 1 μs

The lower limit of the coincidence time window was confirmed to be 0.3 μs, while the upper limit remains unknown. Coincidence operation with a larger coincidence time window was then executed to compare the performance at the coincidence spectrum. The coincidence count rates of different coincident time windows are shown in figure 5.7 below.

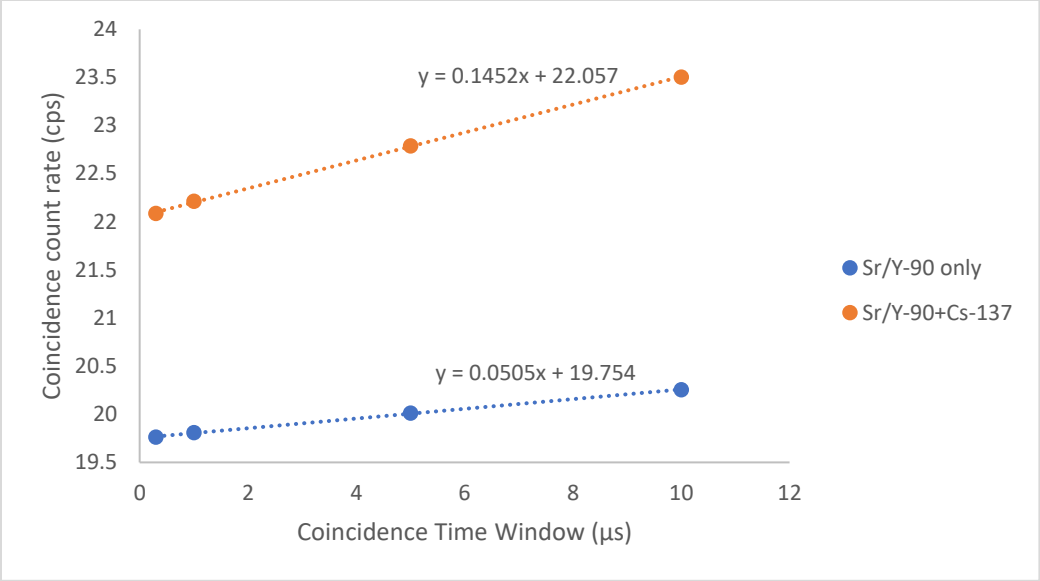

Figure 5.7 Coincidence count rate with different time windows for Beta source (Sr/Y-90) and Beta/Gamma mixed source (Sr/Y-90+Cs-137)

With the increase of the coincidence time window, the event count rate also slowly increases. The majority of the silicon event arrived at the digitizer within 0.3 µs after the signal of the plastic scintillator, and some extra events were considered as coincidence events when the coincidence time window was larger than 0.3 µs. Figure 5.7 indicates that the slope of the coincidence count rate for the beta source (Sr/Y-90) is steeper than the beta/gamma mixed source (Sr/Y-90+Cs-137). With the increase of the coincidence time window, more gamma events are considered coincidence events, ideally beta.

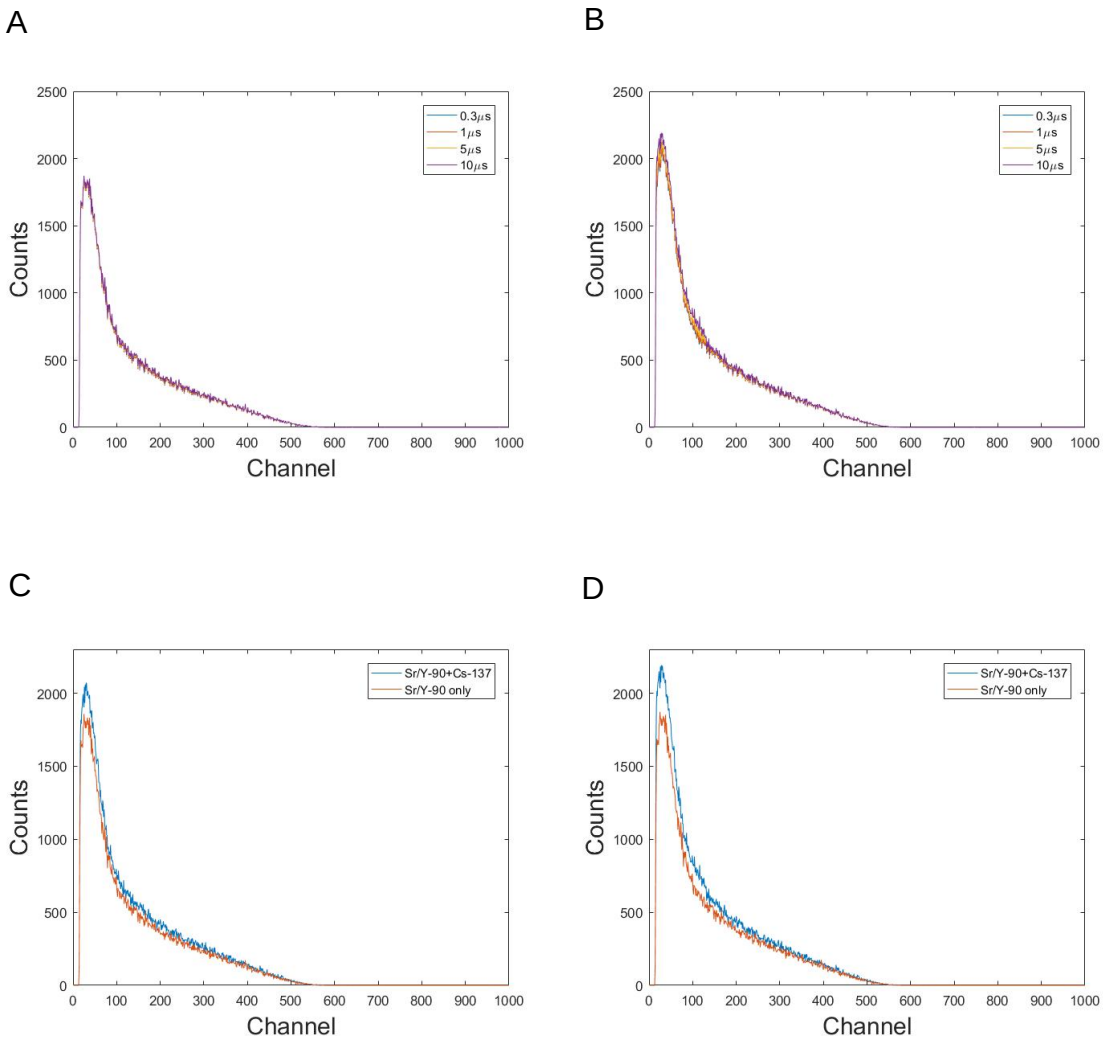

Figure 5.8 Coincidence spectrum with different coincidence time windows for A) Sr/Y-90 source only B) Sr/Y-90 combined with Cs-137. Sr/Y-90 spectrum compared with summed Sr/Y-90 and Cs-137 spectrum for C) 0.3 µs D) 10 µs

Figure 5.8A and 5.8B indicates that the coincidence time window is not the critical parameter for the spectrum. Changing the coincidence time window from 0.3 µs to 10 µs would only increase the coincidence count rate with 2.5% and 6.4% for beta source and beta/gamma mixed source, respectively. The gamma contribution under a larger coincidence time window is significantly higher. Thus, as a higher coincidence time window does not provide enough profit under the

mixed beta/gamma radiation field, a conservative coincidence time window of 0.3 μs was decided for further data analysis.

The coincidence time window would only trigger plastic scintillator events that arrive within 0.3 μs before the silicon event. Accidental and random counts can be neglected considering the higher count rate of the source used in the experiment.

5.4 Coincidence beta spectrum performance for various Beta-Gamma mixed field

The project's motivation is to segregate the beta spectrum from the unknown beta/gamma mixed field under industrial environments. Therefore, the performance of the beta spectroscopy system under various radiation fields would be one of the most notable experiments of the project.

5.4.1 Radiation fields with the different beta to gamma ratios

In the experiment, mixed beta/gamma radiation fields were simulated by changing the distance and geometry of the Sr/Y-90 and Cs-137 sources. The concept of beta to gamma ratio was raised to quantify the composition of the radiation field. The count rate of the plastic scintillator for beta and gamma sources was measured under different distances and geometry; the ratio between those is defined as the beta to gamma ratio. Beta particles emitted from the source could be stopped or scattered before interacting with the plastic scintillator detector; those counts would not be included as the beta events.

Beta source Sr/Y-90 was placed on the holder in front of the detector, where gamma source Cs-137 was placed perpendicular to the detector’s middle axis. Both sources were placed at four different positions to achieve different count rates. The count rates for Sr/Y-90 were controlled to be 50cps, 100cps, 300cps, and 400cps. The count rates for Cs-137 were controlled to be 500cps, 2000cps,

5000cps, and 8000cps. The spectrum of totally 16 different beta-to-gamma ratio from 0.00625(Sr/Y-90:50cps; Cs137:8000cps) to 0.8 (Sr/Y-90:400cps; Cs137:500cps) are collected with coincidence operation.

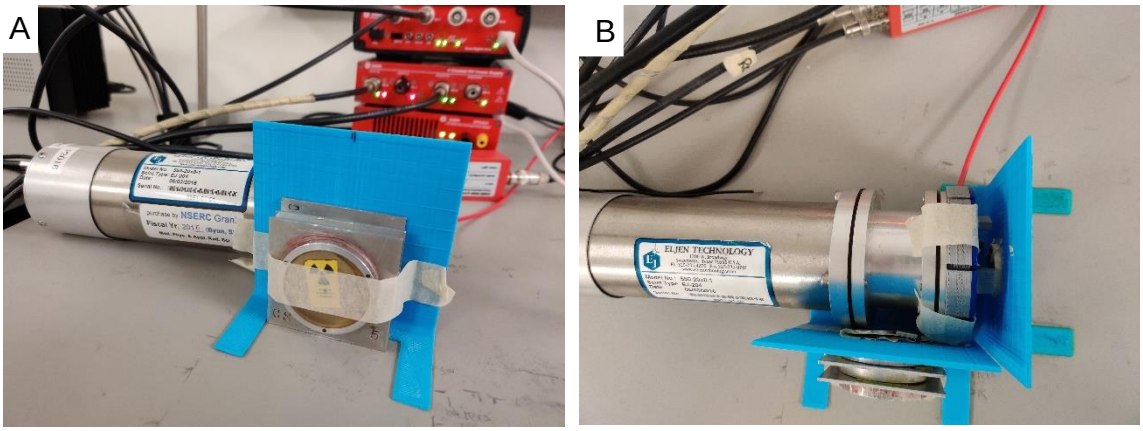

Figure 5.9 Detector and source geometry of the experiment in A) Lateral B) Superior view.

5.4.2 Coincidence spectra

The total and coincidence spectra for the minimum count rate for beta source Sr/Y-90 of 50 cps are shown in Figure 5.10. The beta to gamma ratio in this group would also be minimum when applying the same gamma count rate. The average coincidence count rate is 1.154±0.125 cps. The percentage of range (maximum count rate-minimum count rate/average count rate) is 27.3%. Figure 5.10B suggests that a significant coincidence count rate occurs with the increase of the Cs-137 count rate. The coincidence spectrum's gamma contribution in low energy channels of Sr-90 branch also sharply rise under radiation field with high gamma count rate.

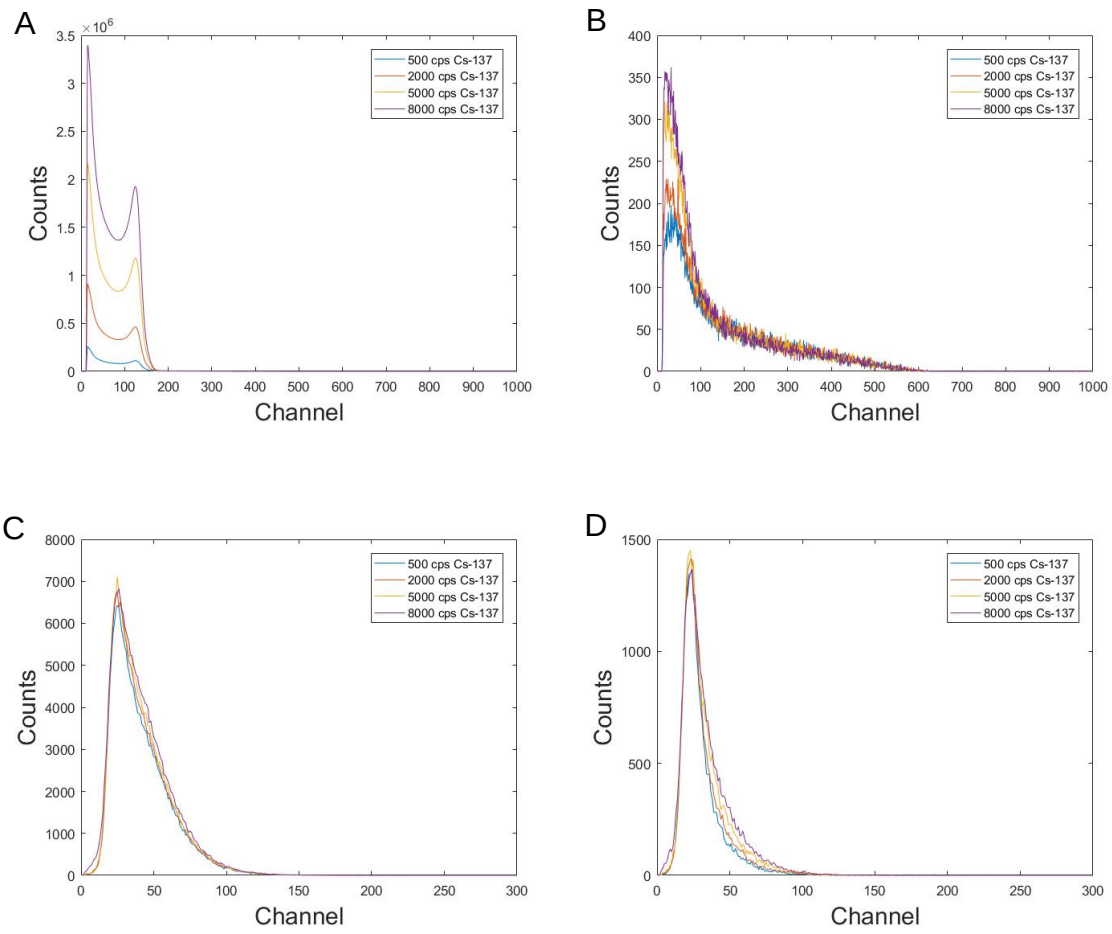

Figure 5.10 Experimental total and coincidence counts for Sr/Y-90 with 50 cps count rate Sr/Y-90 100 cps A) plastic scintillator total counts B) plastic scintillator coincidence counts C) silicon SBD total counts D) silicon SBD coincidence counts

The next count rate of Sr/Y-90 is 100 cps. The total and coincidence spectrum is shown in figure 5.11. The average coincidence count rate is 2.691±0.170 cps. The percentage of the range is 14.0%. The gap of coincidence counts in the lower energy channel of the coincidence spectrum of the plastic scintillator (Figure 5.11B) is smaller than the previous coincidence spectrum of Figure 5.10B.

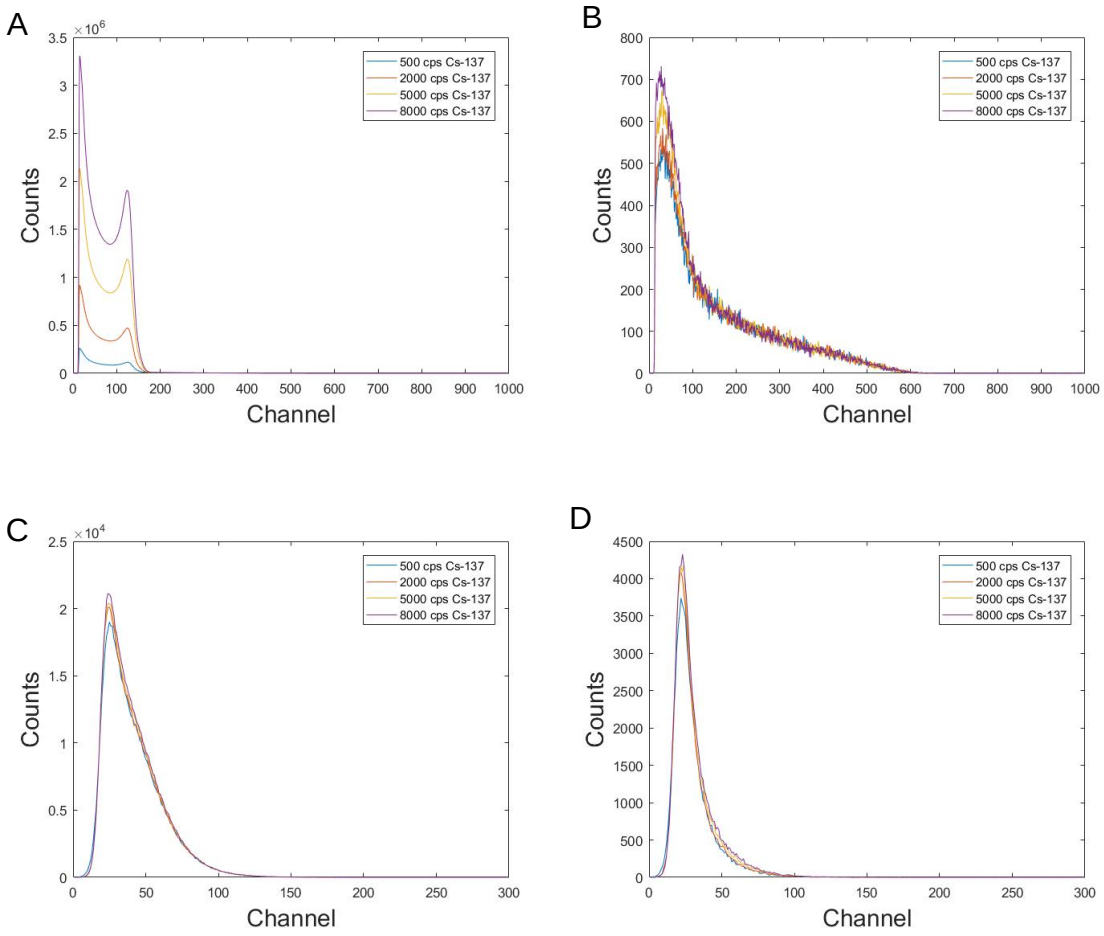

Figure 5.11Experimental total and coincidence counts for Sr/Y-90 with 100 cps count rate A) plastic scintillator total counts B) plastic scintillator coincidence counts C) silicon SBD total counts D) silicon SBD coincidence counts

The total and coincidence spectrum of 300 cps count rate Sr/Y-90 is shown in Figure 5.12 below. The average coincidence count rate is 13.244±0.406 cps, while the percentage of the range is 5.9%. Compared to the coincidence spectrum of lower beta count rate, the coincidence count rate increase, and the percentage of range decreases. The gap of coincidence counts in the lower energy channel of the coincidence spectrum of the plastic scintillator (Figure 5.12B) shirked continuously.

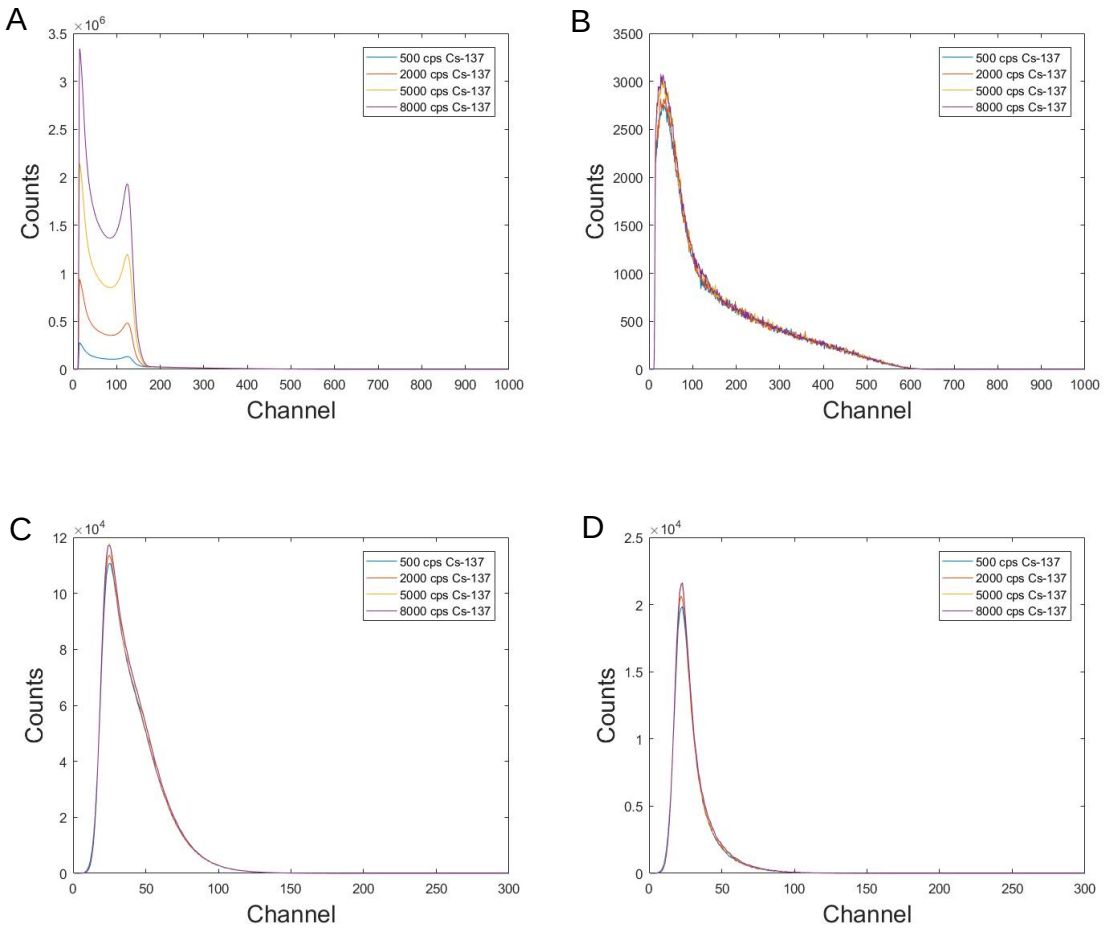

Figure 5.12 Experimental total and coincidence counts for Sr/Y-90 with 300 cps count rate A) plastic scintillator total counts B) plastic scintillator coincidence counts C) silicon SBD total counts D) silicon SBD coincidence counts

Finally, the total and coincidence spectrum of 400 cps count rate Sr/Y-90 is shown in Figure 5.13 below. The average coincidence count rate is 22.962±0.388 cps, while the percentage of the range is 3.5%. This group of data is collected under the radiation field of the highest beta to gamma ratio. The coincidence spectrum of plastic scintillators almost overlaps with each other no matter how high the count rate of Cs-137 is. The drop of standard deviation and percentage of the range also indicates that the system's performance is stable under various radiation fields.

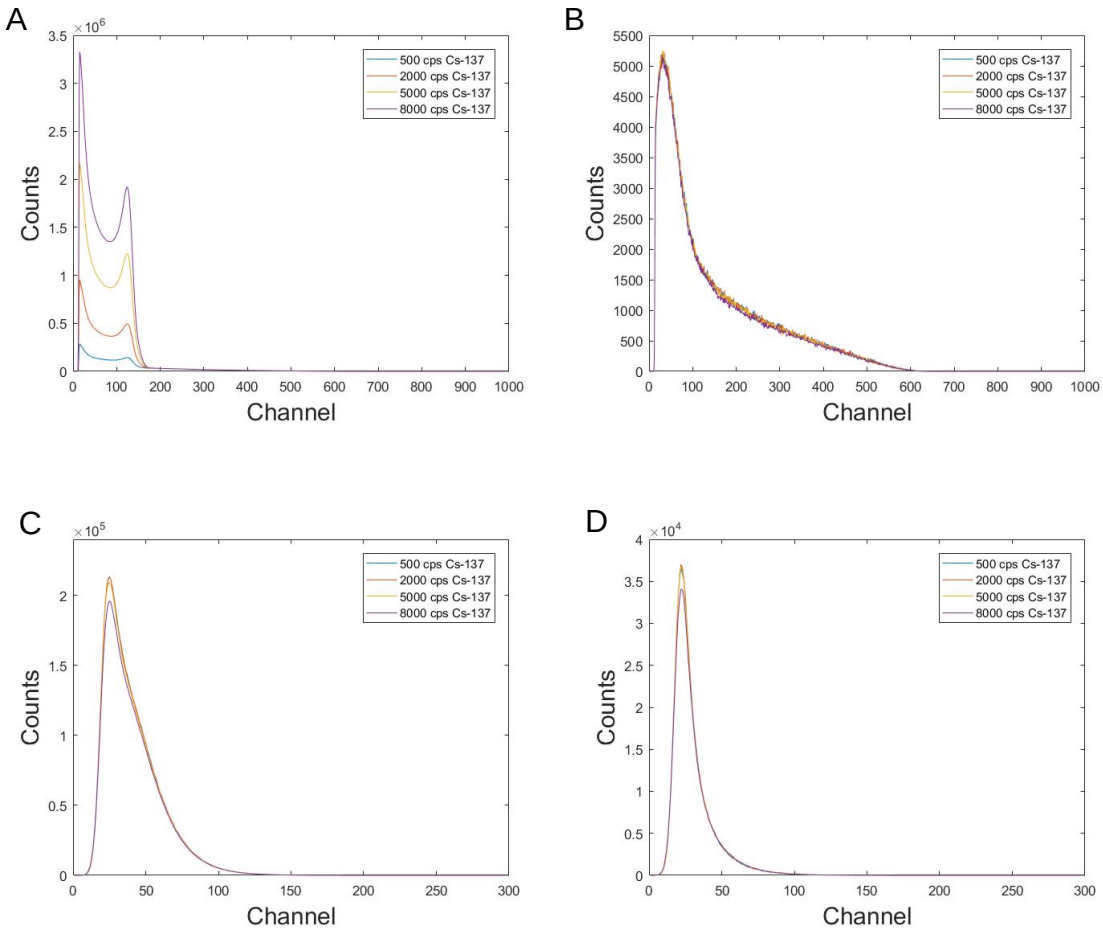

Figure 5.13 Experimental total and coincidence counts for Sr/Y-90 with 400 cps count rate A) plastic scintillator total counts B) plastic scintillator coincidence counts C) silicon SBD total counts D) silicon SBD coincidence counts

5.4.3 Discussion

The coincidence count rate of each measurement is listed below in table 5.6. The increase of the Cs-137 generally increases the coincidence count to a different extent except when the Sr/Y-90 count rate is 400 cps. The trend indicates that more gamma event was considered as coincidence event unlikely. The percentage of the range of four data groups with fixed Sr/Y-90 counts rate varies to a relatively large extent. Increasing the Sr/Y-90 count rate would decrease the percentage of range and stabilize the coincidence spectrum.

Table 5.6 Coincidence count rate of each measurement with different Sr/Y-90 and Cs-137 count rates.

Sr/Y-90 Count rate(cps) / Cs-137 Count rate(cps)	50	100	300	400
500	0.877	2.517	12.821	23.149
2000	0.950	2.590	12.974	23.191
5000	1.081	2.764	13.580	23.127
8000	1.154	2.894	13.602	22.381
Percentage of range (%)	27.3	14.0	5.9	3.5
Average Count rate(cps)	1.015	2.691	13.244	22.962
Standard Deviation	0.125	0.170	0.406	0.388

Ideally, the coincidence count is purely composed of beta events. However, the contamination of the gamma event is inevitable. The coincidence count rate of each measurement was then divided by the Sr/Y-90 count rate performed. The quantity is a “conversion factor,” showing how much coincidence count would be produced when applying one beta event. Figure 5.14 below shows the “conversion factor” for all measurements. The slope of the linear fit line decreased with the increase of the Sr/Y-90 count rate, which confirmed that gamma contribution is dropping to near zero under the radiation field of high beta count rate. A Higher Sr/Y-90 count rate also results in a higher value of the “conversion factor”, meaning that each beta event is more likely to become a coincidence event, thus producing a more precise coincidence spectrum.

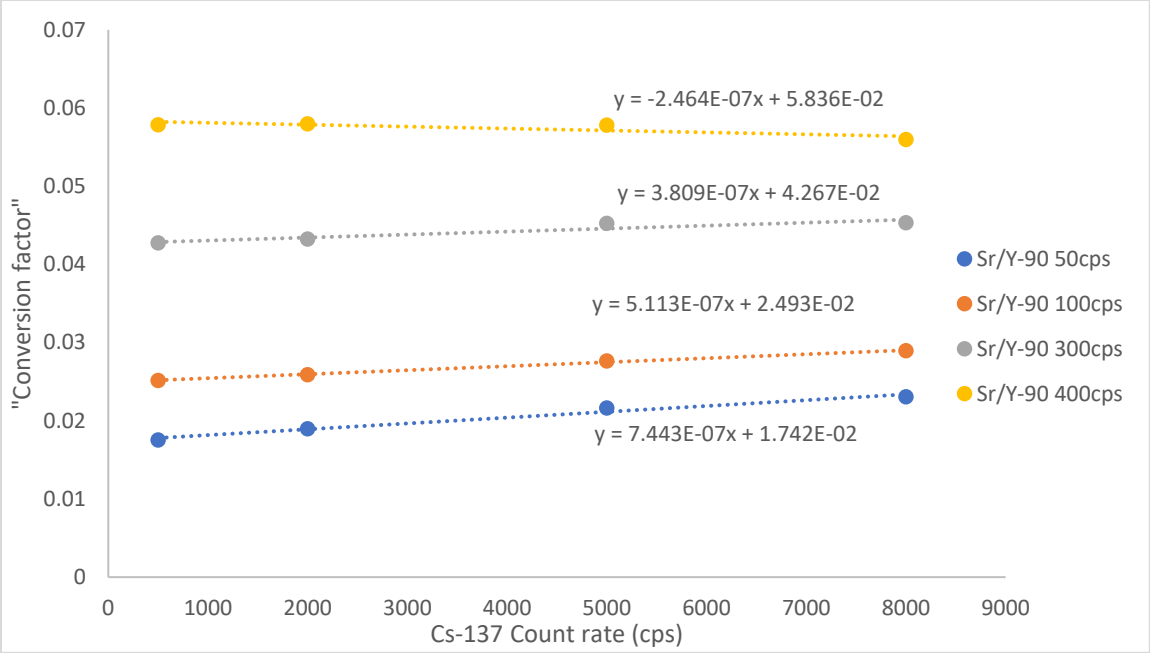

Figure 5.14 The "Conversion factor" of each measurement. (Coincidence count rate/Sr/Y-90 count rate)

The coincidence spectra of the plastic scintillator are normalized to inspect the shape, shown in Figure 5.15. Noticeable spectrum shape differences can be observed in Figures 5.15A and 5.15B. Under the radiation field of higher gamma radiation, more events are gathered at the Sr branch of the coincidence spectrum of the lower channel (lower than channel 100). The shape of spectra further indicates that additional coincidence events from gamma contribution are mainly located at the lower energy range. When the count rate of beta events rose, the coincidence spectra became more similar no matter the gamma count rate; thus, the gamma contribution can be neglected.

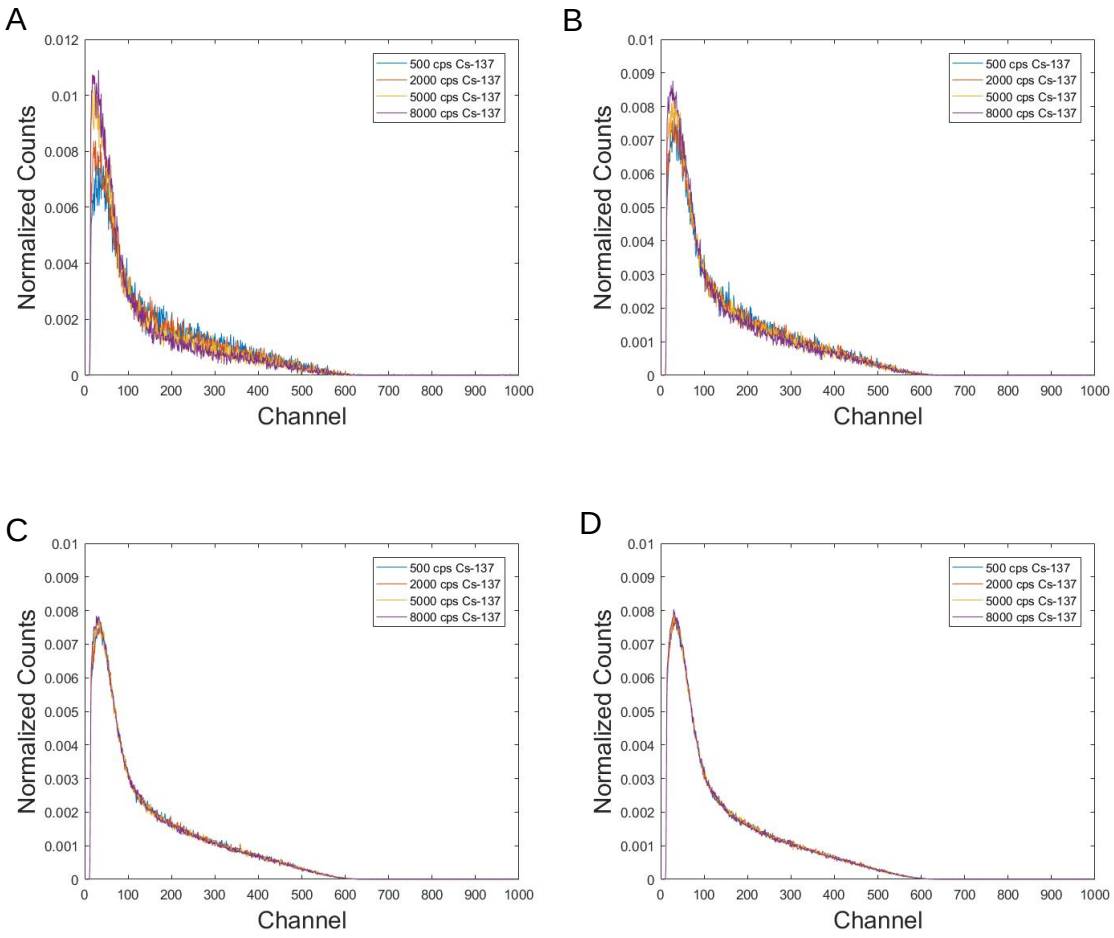

Figure 5.15 Normalized coincidence spectrum of plastic scintillator at the Sr/Y-90 count rate of A) 50 cps B) 100 cps C) 300 cps D) 400 cps

Finally, the integral of the coincidence spectra is calculated by summing the energy corresponding to the channel of each coincidence event. The integral over the whole spectrum indicates the total deposited energy for all coincidence events. All calculated results are listed in Table 5.6 below. Compared to table 5.6 of the coincidence count rate, the range percentage significantly drops for groups at a lower Sr/Y-90 count rate. The table indicates that total deposited energy for a coincidence event is less affected despite a more significant change of the coincidence count rate.

Table 5.7 Total deposited energy of coincidence events of each measurement with different Sr/Y-90 and Cs-137 count rates.

Sr/Y-90 Count rate(cps) / Cs-137 Count rate(cps)	50	100	300	400
500	1.46E+04	4.13E+04	2.06E+05	3.64E+05
2000	1.50E+04	4.18E+04	2.08E+05	3.64E+05
5000	1.54E+04	4.29E+04	2.15E+05	3.59E+05
8000	1.57E+04	4.38E+04	2.14E+05	3.46E+05
Percentage of range (%)	7.2%	5.9%	3.8%	5.1%
Average deposited energy (MeV)	1.52E+04	4.25E+04	2.11E+05	3.58E+05
Standard Deviation	4.79E+02	1.12E+03	4.56E+03	8.60E+03

Chapter 6 Conclusion and future direction

6.1 Conclusion

A series of software and hardware upgrades were conducted to improve the performance of the beta-ray coincidence spectrometer. The data acquisition software was replaced from MC2 to CoMPASS, which has better stability and functionality. Optimal shaping parameters were re-determined following the instruction of the software's user manual.

The PMT signal was modified with several different approaches to have a longer decay time. Benchmark tests of different setups show that except adding a capacitor to the digitizer, both the method of changing the digitizer and adding a preamplifier slowed down the PMT signal. Due to the importance of portability, changing the digitizer was decided to be the final solution.

The coincidence time window was affected by the system changing. A coincidence time window of 0.3 μs was determined from the plotting time graph between silicon and plastic scintillator events. Experiments with mixed beta and gamma sources show that the increase of the coincidence time window would increase the chance that gamma events been recognized as coincidence events, which is unpreferred.

The response of the beta-ray coincidence spectrometer was characterized under the mixed beta/gamma radiation field with various count rate ratios from 0.00625 to 0.8. A higher beta count rate leads to more stable coincidence spectra no matter the gamma count rate, and thus, the gamma contribution can be neglected. However, at the lower beta count rate, coincidence counts at low energy channels are relatively easily contaminated by gamma events. The change of gamma events combines with an evident change of coincidence spectrum in this case.

6.2 Future work

The system components, including both the software and hardware, have excellent and stable performance under various radiation fields. However, the preamplifier's gain for silicon SBD is still too high to display the spectrum with an appropriate energy range. The changing of silicon SBD preamplifier would finish the whole beta spectrometer system.

On the simulation side, more complicated geometry of the detector and sources should be modeled to validate further experiments. Coincidence spectrum simulating with MCNP is the critical part of future simulation work, which should be achieved by the built-in function of PTRAC (particle tracking output).

Experiments under beta/gamma mixed field can also be expanded to more complex geometry and composition of the sources. Currently, all measurements are executed under lab circumstances. The beta measurement inside an ambient gamma field should be performed at CANDU reactors to access actual data. Given the better performance under a higher beta count rate, the radiation field should be estimated before the measurement.

Reference

[1] Canadian Nuclear Safety Commission (CNSC), 2012. Introduction to Dosimetry, INFO-08627. Available from: https://nuclearsafety.gc.ca/pubs_catalogue/uploads/INFO-0827-Introduction-to-Dosimetry-e.pdf

[2] G. Chodick et al., "Risk of cataract after exposure to low doses of ionizing radiation: a 20-year prospective cohort study among US radiologic technologists," Am J Epidemiol, vol. 168, no. 6, pp. 620–631, Sep. 2008, doi: 10.1093/aje/kwn171.

[3] S. Bouffler, E. Ainsbury, P. Gilvin, and J. Harrison, "Radiation-induced cataracts: the Health Protection Agency's response to the ICRP statement on tissue reactions and recommendation on the dose limit for the eye lens," J. Radiol. Prot., vol. 32, no. 4, pp. 479–488, Nov. 2012, doi: 10.1088/0952-4746/32/4/479.

[4] C. Thome, D. B. Chambers, A. M. Hooker, J. W. Thompson, and D. R. Boreham, "Deterministic Effects to the Lens of the Eye Following Ionizing Radiation Exposure: is There Evidence to Support a Reduction in Threshold Dose?," Health Physics, vol. 114, no. 3, pp. 328–343, Mar. 2018, doi: 10.1097/HP.0000000000000810.

[5] E. A. Ainsbury et al., "Radiation Cataractogenesis: A Review of Recent Studies," Radiation Research, vol. 172, no. 1, pp. 1–9, 2009, doi: 10.1667/RR1688.1.

[6] Authors on behalf of ICRP et al., "ICRP publication 118: ICRP statement on tissue reactions and early and late effects of radiation in normal tissues and organs--threshold doses for tissue reactions in a radiation protection context," Ann ICRP, vol. 41, no. 1–2, pp. 1–322, Feb. 2012, doi: 10.1016/j.icrp.2012.02.001.

[7] International Atomic Energy Agency (IAEA), 2014. Implications for Occupational Radiation Protection of the New Dose Limit for the Lens of the Eye, IAEA-TECDOC-1731.

[8] P. W. and G. S. C. Government of Canada, "Canada Gazette, Part 1, Volume 153, Number 24: Regulations Amending Certain Regulations Made Under the Nuclear Safety and Control Act (Radiation Protection)," Jun. 15, 2019. https://canadagazette.gc.ca/rp-pr/p1/2019/2019-06-15/html/reg4-eng.html (accessed Sep. 27, 2021).

[9] R. Behrens and G. Dietze, "Monitoring the eye lens: which dose quantity is adequate?," Phys. Med. Biol., vol. 55, no. 14, pp. 4047–4062, Jul. 2010, doi: 10.1088/0031-9155/55/14/007.

[10] Y. S. Horowitz, C. R. Hirning, P. Yuen, and M. Aikens, "Beta ray spectroscopy based on a plastic scintillation detector/silicon surface barrier detector coincidence telescope," Nuclear Instruments and Methods in Physics Research Section A: Accelerators, Spectrometers, Detectors and Associated Equipment, vol. 338, no. 2, pp. 522–533, Jan. 1994, doi: 10.1016/0168-9002(94)91337-4.

[11] J. Atanackovic, A. R. Hanu, and S. H. Byun, "Eye lens dosimetry in Canadian CANDU nuclear power plants based on operational dosimetric quantities $H_p(10)$ and Hp(0.07)," Applied Radiation and Isotopes, vol. 177, p. 109902, Nov. 2021, doi: 10.1016/j.apradiso.2021.109902.

[12] F. Bohra, J. Atanackovic, S. H. Byun, A. R. Hanu, and A. Laranjeiro, "Quantification of pure beta spectra in mixed beta gamma fields as part of eye lens dosimetry at CANDU power plants," Applied Radiation and Isotopes, vol. 174, p. 109746, Aug. 2021, doi: 10.1016/j.apradiso.2021.109746.

[13] Laranjeiro, A. 2018. The Characterization and Optimization of a LaBr3(Ce) Spectroscopy System for High-rate Spectrometry at CANDU Reactors (Master's thesis).

[14] Bohra, F. 2018. Measurement and Analysis of Beta-ray Spectra at the Ontario Power Generation and Bruce Power CANDU reactors (Master's thesis).

[15] Omar-nazir, L. 2019. Development of a Si-plastic Scintillator Coincidence Beta-ray Spectrometer (Master's thesis).

[16] “EJ-200, EJ-204, EJ-208, EJ-212 - Plastic Scintillators - Eljen Technology.” https://eljentechnology.com/products/plastic-scintillators/ej-200-ej-204-ej-208-ej-212

[17] D Series Planar Totally Depleted Silicon Surface Barrier Radiation Detector | AMETEK ORTEC. Available from: https://www.ortec-online.com/products/radiation-detectors/silicon-charged-particle-radiation-detectors/si-charged-particle-radiation-detectors-for-research-applications/d-series

[18] CAEN,2017, User Manual UM3246 DT5724 2/4 Channel 14bit 100 MS/s Digitizer Rev. 12 - January 27th, 2017

[19] CAEN,2014, User Manual UM3188 DT5781 Dual/Quad Digital MCA Rev. 0 - 03 June 2014

[20] CAEN, 2019, User Manual UM3182 MC2Analyzer User Manual Software for digital Multi Channel Analyzer Rev.10

[21] Guide GD6300 CoMPASS Quick Start Multiparametric DAQ Software for Physics Applications. Rev. 14

[22] CAEN, 2021. User Manual UM5960 CoMPASS Multiparametric DAQ Software for Physics Applications. Rev. 14

[23] CAEN, 2021, DS2634 A1424 Scintillation Preamplifier Data Sheet

[24] “Beta Radiation Standards and Check Sources - for sale.” https://www.drct.com/dss/sources/betasources.htm

[25] “Gamma Disc Sources - Calibration Standards.” https://www.drct.com/dss/sources/gammasources.htm

[26] RADAR Decay Data. Available from: https://www.doseinfo-radar.com/RADARHome.html

[27] R. M. Jr, C. Gesh, R. Pagh, R. Rucker, and R. W. Iii, “Compendium of Material Composition Data for Radiation Transport Modeling,” p. 375.

[28] S. Arfaoui, C. Joram, and C. Casella, “Characterisation of a 90Sr based electron monochromator,” p. 26.

Appendix

MATLAB Coincidence Code

```
close all
clear all

coinw = 0.3*1000000 %convert unit from us to ps
ch=1:1:1024;
ch=ch'
edges = [0:1:1024];
%%
S1 = readtable('Si_.csv');%Read the csv file from CoMPASS
Si_T_0=S1(:,1);%Time read from table, in ps
Si_E_0=S1(:,2);%Energy read from table, in channal
Si_T = table2array(Si_T_0);
Si_E = table2array(Si_E_0);%Convert table to array
indices1 = find(Si_E>0); %Find the event of zero energy
Si = Si_T(indices1);
Si_E_nonzero = Si_E(indices1);

S2 = readtable('Pla_.csv');%Read the csv file from CoMPASS
Pla_T_0=S2(:,1);%Time read from table, in ps
Pla_E_0=S2(:,2);%Energy read from table, in channal
Pla_T = table2array(Pla_T_0);
Pla_E = table2array(Pla_E_0);%Convert table to array
indices2 = find(Pla_E>0); %Find the event of zero energy
Pla = Pla_T(indices2);
Pla_E_nonzero = Pla_E(indices2);
%%
```

```
indices = find(Pla>Si(1));
PlagreaterthanSi = Pla(indices); %values of Pla greater than first element of Si
Pla_E_nonzero2=Pla_E_nonzero(indices);
Si_idx = discretize(PlagreaterthanSi, [Si; Inf]);%find the index of the Si element
that is immediately smaller than the corresponding Pla element
Si(length(Si)+1) = Si(length(Si))
Pldiff = abs(PlagreaterthanSi - Si(Si_idx+1)); %difference between Pl and Si
element that is smaller
Siz= size(Pldiff)
s=Siz(1)
for t = 1:s-1
    if Pldiff(t+1)-Pldiff(t)>=0;
        mindiff(t)=Pldiff(t);
    else mindiff(t)=coinw+1;
    end
end
Pltokeep = mindiff <= coinw; %elements in Pl that are less than coincidence
window after Si
Pltokeep(length(Pltokeep)+1) = 0;
Pltokeep=Pltokeep';
PlAfterCoincW = PlagreaterthanSi(Pltokeep);
Si_corresponding = Si(Si_idx(Pltokeep)+1); %values of time for Si
Si_coinc_idx = Si_idx(Pltokeep)+1; %index of coincidences in Si
Pl_corresponding = PlagreaterthanSi.*Pltokeep;
Pl_corresponding(Pl_corresponding==0) = [];
Tdiff=(Si_corresponding-Pl_corresponding)/1000000
Pladiffus=Pldiff/1000000

Si_coinc_energy = Si_E_nonzero(Si_coinc_idx); %Si coincidence energies
Pl_coinc_energy = Pla_E_nonzero2.*Pltokeep;
```

```
Pl_coinc_energy(Pl_coinc_energy==0) = []; %Pl coincidence energies with
zeroes removed
%%
Pl_total_counts_ = histcounts(Pla_E_nonzero,edges);
Si_total_counts_ = histcounts(Si_E_nonzero,edges);
Pl_coinc_counts_ = histcounts(Pl_coinc_energy,edges);
Si_coinc_counts_ = histcounts(Si_coinc_energy,edges);
```

MCNP Input File

```
c cell card
   1     2    -2.7 -1 3 4 111  $Al case left lid
   2     2    -2.7 -2 4 5  $Al case main part
   3   246   -1.08 -3  $Mylar
 100     1  -1.023 -4  $EJ204
   5   182   -1.19 -5  $light guide
   6     2    -2.7 -7 9  $PMT tube shell
   7   143    -2.6 -9 8  $PMT window,borosilicare glass
   8     0        -8  $inside PMT
 200   281   -2.33 -10  $Si
  10     3   -1.21 -11 12  $PLA holder
  11   246   -1.08 -13  $mylar
  12   210   -2.46 -20 -21 22  $source
  13   246   -1.08 -20 -23 21  $source mylar
1000     4 -0.001205 -100 #1 #2 #3 #100 #5 #6 #7 #8 #200 #10 #11 $region of
          #12 #13
1010     0         100  $outside of interest

c surface card
   1       rcc 0 0 -0.53 0 0 0.947 3.8  $Al case left lid
```

```
 111       rcc 0 0 -0.53 0 0 0.53 2.765  $Al case left lid inner part
   2       rcc 0 0 0.417 0 0 3.583 2.56  $Al case main body for EJ204 and acryl
   3       rcc 0 0 0 0 0 0.000869 2.765  $Mylar
   4       rcc 0 0 0.000869 0 0 2 2.5  $scintillator EJ204
   5       rcc 0 0 2.000869 0 0 2 2.5  $light guide acrylic
   7       rcc 0 0 4.000869 0 0 11.2 2.6  $PMT tube outside
   8       rcc 0 0 4.300869 0 0 10.84 2.38  $PMT tube inside
   9       rcc 0 0 4.000869 0 0 11.14 2.54  $PMT window
  10       rcc 0 0 -1.18 0 0 0.01 0.4  $Si
  11       rcc 0 0 -1.83 0 0 1.3 3.8  $PLA holder outer
  12       rcc 0 0 -1.83 0 0 1.3 0.4  $PLA inner
  13       rcc 0 0 -1.83 0 0 0.000869 0.4  $mylar
  20        cz 1.02  $ volume source radius
  21        pz -2.03  $ source front
  22        pz -2.06  $ source back
  23        pz -2.0236  $ source mylar
 100        so 50  $region of interest, air

mode  e
m246  1000.          0.363632  $mylar
     6000.          0.454552 8016.          0.181816
m4    6000.          0.00015  $air
     7000.          0.784431 8000.          0.210748 18000.         0.004671
m2    13000.               1  $al
m182  1000.          0.53332  $acrylic
     6000.          0.333345 8000.          0.133335
m281  14000.               1  $Si
m143  5000.          -0.0213  $glass boron
     8000.          -0.4806 11000.          -0.0045 13000.          -0.0762
     14000.          -0.2577 25000.          -0.0254 20000.          -0.1265
     9000.          -0.0021 22000.          -0.0034 26000.          -0.0023
```

```
m1    1000.          0.5239  $EJ204
      6000.          0.4761
m3    1000.          0.4445  $PLA
      6000.          0.3333 8000.          0.2222
m210  39000.             -1  $ yttrium
imp:e   1 13r       0           $ 1, 1010
sdef  pos=0 0 -2.02998 erg=d1 vec=0 0 1 dir=d2 axs=0 0 1 rad=d3 ext=d4
si1 H 0 0.01365 0.04095 0.06825 0.09555 0.12285
       0.15015 0.17745 0.20475 0.23205 0.25935
       0.28665 0.31395 0.34125 0.36855 0.39585
       0.42315 0.45045 0.47775 0.50505 0.53235
sp1 D 0 0.0778509 0.0760249 0.0749526 0.0740254 0.0729991
       0.0717431 0.07012   0.0680344 0.0653356 0.0619411
       0.0557551 0.0527167 0.0467696 0.0400685 0.032672
       0.0248447 0.0171045 0.00975013 0.00428474 0.00100701
si2 0 1
sp2 -21 0
si3 0 1.02
sp3 -21 1
si4 0 0.00002
sp4 -21 0
f18:e 100 200
*f28:e 100 200
e0 0 1022I 2.5
ft18 geb 0 0.1 0 $ gaussian energy broadening
ptrac file=asc write=all type=e cell=100,200 event=col,sur,src max=1e6
nps 1e6
```